"Simulation Facets in Theory and Technology of Superplastic Forming": Monograph.
The analytical model of superplastic forming (SPF) of spherical shells by pressure of gas generated during sublimation of a sublimating agent is presented. The control of temperature distribution over the surface of the AlMg6 blank by sublimated substances is proposed. It is proposed to describe the contour of the sheet billet at all stages of SPF by universal equations "superformula" and "super ellipse". The dependence of the values of principal stresses on the principal radii of curvature and thinning of shells during superplastic forming has been established. Modeling of superplastic deformation processes of optically transparent materials based on diene and vinyl aromatic hydrocarbons is proposed. The fundamental possibility of using the tungsten-free CrNi73CuBeTeAl alloy, obtained both by vacuum-arc remelting and electroslag remelting, as a tooling material of dies for SPF and isothermal stamping has been shown.

V.V. KUKHAR – D.Sc., Prof., Vice-Rector for R&D Work, Technical University "METINVEST POLYTECHNIC", Ukraine.
O.S. ANISHCHENKO – Ph.D., Ass. Prof. of the Dep. of Metalforming, Pryazovskyi State Technical University, Ukraine.
I.V. VISHTAK – Ph.D., Ass. Prof. of the Dep. of Life Safety & Safety Pedagogy, Vinnytsia National Technical University, Ukraine.

9 786205 511527

Volodymyr V. KUKHAR
Oleksandr S. ANISHCHENKO
Inna V. VISHTAK

SIMULATION FACETS IN THEORY AND TECHNOLOGY OF SUPERPLASTIC FORMING

Monograph

LAP LAMBERT Academic Publishing

Volodymyr V. KUKHAR
Oleksandr S. ANISHCHENKO
Inna V. VISHTAK

SIMULATION FACETS IN THEORY AND TECHNOLOGY OF SUPERPLASTIC FORMING

Volodymyr V. KUKHAR
Oleksandr S. ANISHCHENKO
Inna V. VISHTAK

SIMULATION FACETS IN THEORY AND TECHNOLOGY OF SUPERPLASTIC FORMING

Monograph

LAP LAMBERT Academic Publishing

Imprint
Any brand names and product names mentioned in this book are subject to trademark, brand or patent protection and are trademarks or registered trademarks of their respective holders. The use of brand names, product names, common names, trade names, product descriptions etc. even without a particular marking in this work is in no way to be construed to mean that such names may be regarded as unrestricted in respect of trademark and brand protection legislation and could thus be used by anyone.

Cover image: www.ingimage.com

Publisher:
LAP LAMBERT Academic Publishing
is a trademark of
Dodo Books Indian Ocean Ltd. and OmniScriptum S.R.L Publishing group
Str. Armeneasca 28/1, office 1, Chisinau-2012, Republic of Moldova, Europe
Printed at: see last page
ISBN: 978-620-5-51152-7

Volodymyr V. KUKHAR
Oleksandr S. ANISHCHENKO
Inna V. VISHTAK

SIMULATION FACETS IN THEORY AND TECHNOLOGY OF SUPERPLASTIC FORMING

Monograph

2022

AUTHORS: **Volodymyr V. KUKHAR –** D.Sc. (Eng.), Professor
Vice-Rector for R&D Work, Technical University "METINVEST POLYTECHNIC", Ukraine

Oleksandr S. ANISHCHENKO – Ph.D. (Eng.), Senior Research Associate, Associate Professor of the Department of Metalforming,
Pryazovskyi State Technical University, Ukraine

Inna V. VISHTAK – Ph.D. (Eng.), Associate Professor, Associate Professor of the Department of Life Safety and Safety Pedagogy, Vinnytsia National Technical University, Ukraine

REVIEWERS: **Volodymyr V. Drahobetskyi** – D.Sc. (Eng.), Professor, Kremenchuk Mykhailo Ostrohradskyi National University, Ukraine

Oleg E. Markov – D.Sc. (Eng.), Professor, Donbass State Engineering Academy, Ukraine

Volodymyr V. KUKHAR,
Oleksandr S. ANISHCHENKO,
Inna V. VISHTAK

Simulation Facets in Theory and Technology of Superplastic Forming : Monograph.

The analytical model of superplastic forming (SPF) of spherical shells by pressure of gas generated during sublimation of a sublimating agent is presented. The control of temperature distribution over the surface of the AlMg6 blank by sublimated substances is proposed. It is proposed to describe the contour of the sheet billet at all stages of SPF by universal equations "superformula" and "super ellipse". The dependence of the values of principal stresses on the principal radii of curvature and thinning of shells during superplastic forming has been established. Modeling of superplastic deformation processes of optically transparent materials based on diene and vinyl aromatic hydrocarbons is proposed. The fundamental possibility of using the tungsten-free CrNi73CuBeTeAl alloy, obtained both by vacuum-arc remelting and electroslag remelting, as a tooling material of dies for SPF and isothermal stamping has been shown.

CONTENT

INTRODUCTION

Superplastic forming of metals and alloys (SPF) is the process of making hollow products from sheet blanks, hermetically clamped along the flange between two halves of the die, under the influence of a difference in gas pressure, which is created on both sides of the blank (Fig. 1). The characteristic features of the process are the absence of dynamic loads and the shaping of the product only due to the thinning of the free (not clamped in the stamp) section of the workpiece.

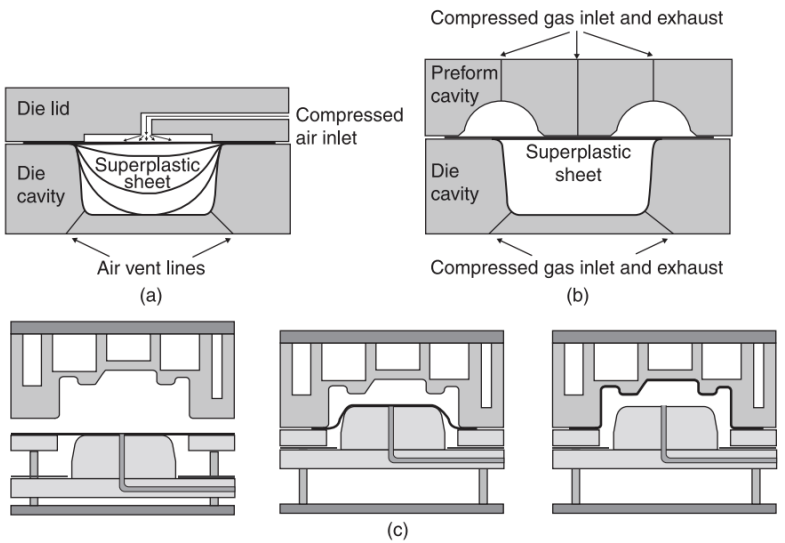

Figure 1. Schematic illustration of different types of SPF dies utilizing: (a) – single-stage forming; (b) – two-stage forming; (c) – double-action forming

SPF was first copied in 1964 from the process of gas forming of thermoplastics [1]. In industry, the most widely used SPF of spherical products without contact of the workpiece with the walls of the matrix (Fig. 1a). In addition, to achieve a uniform wall thickness of products, a two-single reversible SPF is used (Fig. 1b) and an SPF in combination with stamping with a metal punch [2,3]. At the first stage of the SPF (molding in the rift cavity in the upper half of the die in Fig. 1b or preliminary stretching of the workpiece with a metal punch in Fig. 1c), the thickness of the predominantly peripheral sections of the workpiece decreases. In the second stage, during molding by gas pressure, the central zones of the preform are thinned. Thus, the finished product has a uniform wall thickness.

Constant growth in parts and materials range, manufactured by SPF of sheets, including in combination with diffusion welding [2] stipulates the necessity to modify the existing processes and develop new methods for designing of these processes.

The authors presented in the monograph an analytical model of superplastic forming (SPF) of spherical shells by pressure of the gas (gaseous phase) created upon sublimation of sublimate agent. The authors showed that the SPF pressure control can be effectively applied by the way of change in the forming temperature relative to temperature of sublimate agent sublimation. The experimental results of forming of shells from aluminum alloys, confirming theoretical calculations of the velocity and temperature conditions of SPF by the sublimating agent pressure.

Next, the authors studied SPF of non-uniformly heated sheet blanks from aluminum alloy *AlMg6*. To create an uneven temperature field over the surface of the blank, coatings were used from sublimated substances at temperatures 50…150 °C below the SPF temperature (450 °C for *AlMg6* alloy). An aqueous solute of chloride and ammonium iodide having a sublimation temperature at normal pressure and a latent heat of conversion equal to 338 and 404 °C, 330

and 355 kJ/kg, respectively, was sprayed onto the central zones of the blanks. The experiments showed a decrease in the thickness of the shells to be formed up to 4…10 % on the working surface of the shells. SPF in an uneven temperature field distorts the spherical contour of the shells. This increases the calculation error of the SPF process using sublimate pressure.

In this regard, the authors showed in the work that the contour of a sheet blank at all stages of SPF can be described by application of the universal equations known as a "superformula" and "superellipse". The work has the results of approximation by the proposed equations of shell contours that manufactured by SPF by different methods. The application of the “superformula” to approximate the spherical shell contours in the first stage of molding has been tested. The graphs that show the ratio of the ordinates of the contours of the spherical shells and the hemisphere are given. It is shown that the contours of the shells from the *AlMg5* and *Sn*-38%*Pb* alloys are rejected in the direction of the formation of parabolas. It was found that the deviations increase with decreasing the coefficient of high-speed hardening of the alloy of the shell. The contour of *AlMg6* alloy shells and blanks of variable thickness, with maximum in the central zone, is diverted from the hemisphere towards the ellipse. The prospects and novelty of using the expression of Lame's superellipse for approximating the curvature of shells in SPF and for predicting the geometry of a product are shown. Different versions of the SPF facilitate the realization of different radii of curvature of the shell contours, which differ significantly from the radius of the spherical segment. The regularities of the change in the radius of conjugation of the bottom and the wall of the spherical shell for various SPF variants are established.

When using the Lame’s superellipse to describe the curvature of the shells, it was established that the principal stresses, especially the tangential stress, depend on the principal curvature radii. It is shown that the intensity of stresses also depends on the thinning of the

shells during superplastic forming. It is revealed that the higher the level of superplastic properties of the material of the blank, the less the principal stresses and effective stresses depend on the difference between the principal radii of curvature.

It is proposed to simulate the processes of superplastic deformation on optically transparent materials based on diene and vinyl aromatic hydrocarbons, a polar plasticizer and a non-coloring stabilizer. It is shown that the rate hardening coefficient of such materials can vary from 0.2 to 1.0 in the range of superplastic deformation rates.

The fundamental possibility to use the tungsten-free CrNi73CuBeTeAl alloy manufactured of both vacuum arc remelting and electroslag remelting as die tool material for SPF and isothermal die forging is shown. It will be efficient to use such dies for SPF and isothermal die forging of Ti-alloys with rather big allowance on the overall sizes, which assumes residual dies upsetting $\varepsilon = 1.0\text{-}3.0$ % during exploitation. By reducing the complexity of ingot smelting and the ability to make the working face on copiers and milling machines instead of EDM, the dies manufacturing from CrNi73CuBeTeAl alloys will reduce the dies expenses in the blade forgings technological cost from 32 % to 20…22 %.

1. CALCULATION AND VERIFICATION OF SUBLIMING AGENT GAS PRESSURE AT SPF

Superplastic forming of spherical shells from sheets is performed by a gas medium. The application of a gas medium is associated with the use of compressor plants and pipelines that are hermetically sealed into forming dies [3, 4]. An important advantage of superplastic forming is not the use of press equipment and the elimination of a number of problems in the area of ensuring the accuracy of the "press-die" system and occupation safety [5-7].

One of the modern and progressive variants of superplastic forming is the molding of shells by the pressure of a gaseous medium formed as a result of a change in the aggregate state of thermo-metastable substance (sublimate or destruct agent) in the hermetic die cavity [4]. Based on this kind of gas forming, in this work an attempt is made to determine the optimal power regime in relation to free forming of dome-shaped shells due to the controlled sublimation in the die cavity. Preliminary analysis has shown that a sufficiently large number of factors (mass, density, surface area, critical temperature of the sublimate, geometric dimensions of the preform, die, forming temperature, etc.) affecting the formation of domes cause significant difficulties in the experimental determination of optimal gas-forming regimes with controlled sublimation of subliming agent. Therefore, the problem was solved theoretically and tested experimentally with the example of free bulging of workpiece from Magnalium (table 1.1) with a radius of r = 46 mm in a die with a clamping lid with a diameter of D = 92 mm and a height of 135 mm.

Calculation of SPF is based on the theory of momentless shells [8, 9]. The following assumptions are made: deformation is triaxial and axisymmetric; the stress state is flat and axisymmetric, the incompressibility conditions, deformation hardening, elastic deformations, the anisotropy of the mechanical properties of the molded material and dynamic loads are negligibly small. In addition, it was assumed that the thinning of the shell walls is uniform, and the temperature of the die surface on contact with the sublimate layer remains constant and equal to the forming temperature. It was assumed that the heat transfer in the cavity of the die is carried out by radiation, and convection and thermal conductivity can be neglected, due to the absence of communication with the external medium and the formation, upon sublimation, of the gas cushion separating the die walls and the surface of the sublimate in the solid state.

Table 1.1. Chemical composition of magnalium alloys (GOST 4784-97)

Alloy	*Mg*	*Mn*	*Si*	*Fe*	*Cu*	*Cr*	*Zn*	*Ti*	*Al*
AlMg3	3,2-3,8	0,3-0,6	0,5-0,8	<0,5	<0,1	<0,05	<0,2	<0,1	rest
AlMg5	4,8-5,8	0,3-0,8	<0,5	<0,5	<0,1	-	<0,2	0,02-0,1	rest
AlMg6	5.8-6,8	0,5-0,8	<0,4	<0,4	<0,1	-	<0,2	0,02-0,1	rest

As a "reference" law for regulating gas pressure during forming into a cylindrical cavity, the Jovane ratio [10] was chosen:

$$\frac{p}{p_0} = \frac{H(1+H^2)^2}{H_0(1+H^2)^2} \qquad (1.1)$$

where H – relative height of the shell, $H = h/r$ (h is the height of the shell); H_o – initial relative height of the shell; p – forming pressure; p_0 – initial forming pressure corresponding to the height H_o.

The parameters of the formation of H_o and p_o were determined from the known dependences of the mechanics of continuous media and on the basis of the equation for the elastically viscous plastic medium [10]. The increase in forming pressure during sublimation in the die cavity to a maximum, i.e., until the temperature of the sublimation reaches the forming temperature, is described by the combination of the following dependencies:

- the equation of state of a mixture of real gases developed by Berthelot:

$$\frac{dm_g}{\mu_m} R_u T = (V + p)dp + (p + c)dV \tag{1.2}$$

- the chemical equation of the sublimation reaction of sublimate agent arbitrary mass:

$$\mu_M f_M dm_g = \mu_m \sum_{i=1}^{N} f_{m_i} dM \tag{1.3}$$

- the equation of the thermal balance of the sublimation process:

$$F\sigma E(T^4 - T_M^4)d\tau = qdM \tag{1.4}$$

- the Clapeyron-Clausius relation for the sublimation of substances:

$$R_u T_M^2 dp = qpdT_M \tag{1.5}$$

- the ratio that determines the volume of the gaseous phase in the closed die cavity:

$$V = \frac{\pi D^2 l}{4} - \frac{M}{\rho} + \frac{\pi a^3 H(H^2+3)}{6} \tag{1.6}$$

- the equation for calculating the duration of forming at a given optimal strain rate:

$$\xi(1+H^2)d\tau = 2HdH \tag{1.7}$$

- ratio that relating the surface area changing and sublimate agent mass with the thickness of its layer:

$$dF = 4\pi(\alpha+1)S_M dS_M \tag{1.8}$$

$$S_M = \sqrt[3]{\frac{M}{\pi\rho\alpha^2}} \tag{1.9}$$

of which

$$dF = \left[\frac{4\pi(\alpha+1)}{3\sqrt[3]{\pi^2\alpha M\rho^2}}\right] \tag{1.10}$$

In the dependences (1.2) – (1.10): M – mass of the sublimate agent; m_g – mass of the gaseous phase; μ_M, μ_m – accordingly molar masses of the sublimate and mixtures of gases created during its sublimation; R_u – universal gas constant; T – forming temperature; V – volume of the gaseous phase; b, c – correction factors in the Berthelot equation; f_m, f_M – stoichiometric coefficients of the sublimation reaction; T_c – critical temperature of the sublimate agent; F – surface area of the sublimate agent; σ – Stefan-Boltzmann constant; E – reduced degree of blackness of bodies surface; q – latent heat of sublimation; τ – forming time; l – cavity depth of the presser

cap of the die; ρ – density of the sublimate agent; $\alpha = a/S_M$, a, S_M – radius and thickness of the sublimate layer in the die cavity, respectively.

The maximum correspondence of the pressure increase at sublimation of sublimate agent with the ascending branch of the "reference" dependence (1.1) at the section $H_0 \leq H \leq 1/\sqrt{3}$ was established by means of a computer calculation by varying within the specified limits of parameters entering into equations (1.2) – (1.10). At the stage of shell forming with height $H = 1/\sqrt[2]{3}$ necessary pressure decrease was determined by formula (1.5). At the same time, the forming temperature was reduced by shutting down the die heating system, which caused the interfacial equilibrium of the sublimate to equal at forming and sublimation temperatures.

For the experimental verification of the proposed model of gas superplastic forming at all its stages and taking into account the fact that the velocity and temperature ranges of the superplastic deformation of the Magnaliums, $\xi = 10^{-2}$-10^{-4} s^{-1}, $T = 380...450$ ºC, in theoretical calculations the forming temperature was assumed as 450 °C in order to increase the possible range of its change when forming domes in height $H \geq 1/\sqrt{3}$, and the strain rate varied only in the above-mentioned limits in increments of $\Delta\xi = 2 \cdot 10^{-4}$ s^{-1}.

The optimum values of the parameters of the SPF calculated with a computer with a minimum gradient of the strain rate were verificated by forming to crashing the walls of the domes from alloys *AlMg3*, *AlMg5* and *AlMg6* with initial thickness of workpieces $S_o = 0.6...1.0$ mm (when using the sublimate NH_4Cl).

Optimum parameters of the superplastic forming see Table 1.2.

For comparison; chose the ratio of the calculated and experimentally determined by the equation (1.7) deformation rates of shell. Under the experimental conditions (Fig. 1.1), the error of calculation on a computer that smaller than higher the level of superplastic properties of the workpiece material and the greater the

geometric dimensions of the workpiece. S_0, ratio of the theoretical and experimental data for workpiece formed of *AlMg5* alloy with thickness S_0 = 1.0 mm is 2.46.

Table 1.2. Optimum parameters of the SPF

Alloy	M, kg	ξ, s^{-1}	α	V_M, cm^3	S_0, mm
AlMg5	0.9	$8 \cdot 10^{-4}$	1.3	30	1
AlMg6	0.75	$6 \cdot 10^{-4}$	2.25	25	0.6
AlMg3	0.75	$6 \cdot 10^{-4}$	2.25	25	0.6

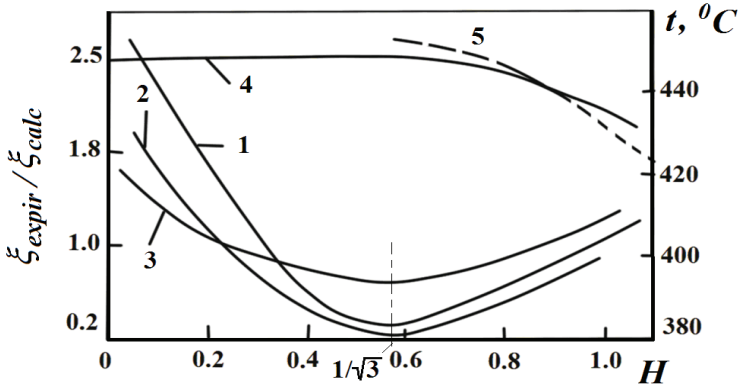

Figure 1.1. Comparison of calculated and experimental values of strain rates (1, 2, 3) and temperature change (4, 5) in process of domes forming, ξ_{expir}, ξ_{calc} – experimental and calculated strain rate: 1 – *AlMg5* alloy; 2 – *AlMg6* alloy; *3* – *AlMg3* alloy; 4 – experimental values of forming temperature; 5 – lowering of temperature (calculated according to the Clapeyron-Clausius equation) at the stage of forming domes with height $H \geq 1/\sqrt{3}$

With a decrease in the relative thickness S_0/r of the workpiece the error is reduced to 1.88 (*AlMg6* alloy) and 0.94 (*AlMg3* alloy). With the same geometric dimensions of the workpieces, the index of the unevenness of the strain rate for the magnesium *AlMg3* is lower than for *AlMg6*.

Despite the high error in the theoretical calculation, the results obtained can be considered satisfactory, since in all experiments the absolute values of the strain rate for shells did not exceed the limits of superplasticity values and amounted: to alloy *AlMg5* is $\xi = 2.16 \cdot 10^{-4}$ … $2.18 \cdot 10^{3}$ s^{-1}; to alloy *AlMg6* $\xi = 1.3 \cdot 10^{-4}$ … $1.3 \cdot 10^{-2}$ s^{-1}; to alloy *AlMg3* $\xi = 5.76 \cdot 10^{-3}$ … $1.33 \cdot 10^{-2}$ s^{-1}.

The decrease in temperature, determined theoretically, as well as its change in the course of experiment, show that at the instant of shell rupture ($H \leq 1.1$) is temperature $T \geq 420$ °C, i.e. the forming temperature was in the optimum range of superplastic deformation for the investigated alloys.

Maximum height of formed shells of *AlMg5*, *AlMg6* and *AlMg3* alloys was increased to 16.2, 21 и 24 % respectively. Increasing the resource of the deformation ability of alloys without significantly complicating of forming technology, applied equipment and rigging testifies to the prospects of industrial use of the proposed mode of SPF.

2. SPF SHELLS FROM SHEET BLANKS WITH SUBLIMATING AND DESTRUCTIVE COATINGS

The main disadvantage of the process of shells SPF from sheet blanks is the large variability of the walls along the contour of products. So the thickness of the wall in the pole ("crown") of the hemisphere varies between 40...70 % of the initial thickness of the blank. There are a number of ways to regulate the metal flow during plastic forming, in particular, elimination of products thickness variability. They provide the preliminary profiling of the blank or semi-finished product, changing the structure of the metal of the blank and the face friction conditions at the "workpiece-die" border, and SPF in an uneven temperature field.

Preforming of semi-finished product is the most common way in the industry to control its thickness [3, 11, 26]. SPF process in this case provides, as a rule, two-stage forming by pneumo-mechanical or reversible forming (RF) methods. The deep drawing by a metal punch with the maximum thinning of the peripheral zones of the blank is added to the gas forming (before or after SPF) with a predominant refinement of the central zones of the blank [12, 27]. As a result, the thickness distribution in the product is close to uniform. RF of shells on the first stage is carried out into the cavity of the rift along its contour, selected in such a way that the zones of the preform near the flange are deformed most intensively. At the second stage, when the gas pressure is reversed, the semi-finished product is formed into the cavity of the die with the predominant thinning of its central part.

Pre-profiling of the initial blanks involves stamping the blanks with an increase in the thickness of the metal in places that are maximally thinning with further SPF [13, 14, 28, 29]. In this case, with

the same strain degrees of the shell, the absolute value of the wall thickness will be close to the wall thickness in the zones of small strain.

The change in the structure of the blank's metal assumes the formation of grains of various sizes in the required places [15, 16, 30, 31]. Most often in preforms with a prepared superplastic structure in the zones with the maximal deformation in the SPF the grain is preliminarily coarsened, for example, by local heating. Later at the SPF these zones are deformed to a lesser degree, which provides a relatively uniform thickness of the products. Information [17, 32] on additional fining of grain in blanks by contact friction methods has appeared which significantly affects the accumulated strain. In this case, the preliminary fining of the grain should be in the zones adjacent to the flange of the blank both when deep drawing.

The non-uniform temperature field (NUTF) in the blanks at SPF is provided by creating a temperature gradient either over the depth of the die or over the surface of the blank [11, 26]. Lowering the temperature in the most thinning zones of the blank inhibits their deformation at SPF in the NUTF, providing a more uniform thickness of the product.

Each ways to control the blank's metal flow at SPF has its drawbacks: the need for an additional forming tool, the reduction in SPF productivity, the cost of preparing the structure, the application and removal of lubricant, etc. We have proposed a new method for regulating of the metal flow at SPF by applying the thermally unstable coatings (sublimates) onto the sheet blank, which, due to a given thermal effect on the blank, changes its temperature field and formed local thicknesses.

Blanks probed $R = 46$ mm, thickness $S_0 = 0.9 \ldots 1.0$ mm *AlMg6* alloy with a grain size 15…20 μm. As thermally unstable coatings used ammonium chloride and ammonium iodide.

Coating in the form of a supersaturated aqueous solution hit on preparations by spray stencils using a spray bottle. The uneven distribution of the thickness of the coating at first approximated by linear function $y = A(r/R)-B$ in the range $0{,}16 \le (r/R) \le 1$ (r – current distance from flange blank to the center; A, B – indices of approximation). Close to the linear distribution of the thickness of the coating was due to the technical abilities of the spray and the limited size of the blank.

Effect of sublimation of ammonium from the surface of the blank thickness products studied for example free blow-molding of crowns with a relative height of $H = 0.6 \ldots 1.0$ in hard-pinched flange. Blank modeled compressed air pressure up to 0.6 MPa at temperatures 450±10 ºC, i.e. within the temperature range of superplastic forming alloy *AlMg6* [11, 26]. The thickness of the blank and sublimates on its surface was measured at BMI-1 microscope. Variability of thickness of the crowns has been shaped by indicator ΔS:

$$\Delta S = \frac{S_{max} - S_{min}}{S_p} \qquad (2.1)$$

where S_{max}, S_{min} – respectively the maximum and minimum wall thickness of the crown; S_p – shell's wall thickness determined conditions of perfectly uniform deformation.

Spreading of thinning membranes evaluated the relative thickness of S/S_p (S – wall thickness of the crown at this point).

On Fig. 2.1 the scheme of forming crowns with a sublimation coating.

The coated blank was heated prior to forming. Upon reaching temperature sublimation the layer of sublimation risen and stabilized temperature plots the blank underneath it at the level of T_c + (20 … 30) ºC, while free from coating the surface of the blank would be heated to the optimal temperature forming the first T. Stage of the process was characterized by low temperature most part blanks,

except the ring zone ($0 \le r/R \le 0.2 \ldots 0.45$) from the flange. Thus provided the most suitable temperature deformation of peripheral sites. As the blow-shell superplastic forming mode distributed at stations presets, am from sublimate, which resulted in a rise in temperature from T_c + (20 …30) °C to T. Hence, inhibition of thinning the blank in time zones carried out in proportion to the reduction of wall thickness during isothermal stamping.

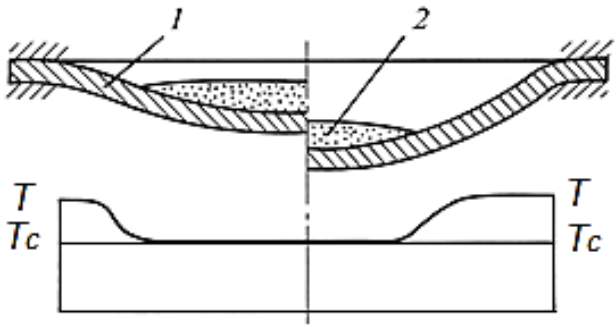

Figure 2.1. Scheme of SPF of crown with subliming coatings:
1 – blank; 2 – coating

Shell height $H < 0.3 \ldots 0.4$ is characterized by sufficient uniform wall thickness [3], therefore, in the initial stages of forming exercised without sublimation coating. For this changed partial pressure above the surface of the sublimate in accordance with the equation of the Clausius-Clapeyron. In the first stages of molding to save sublimate created over its surface pressure, ensuring inequality $T_c > T$. Sublimation was virtually non-existent, and the temperature of all sections of the blank has been tweaked. On reaching the limit crown height of $H = 0.2 \ldots 0.3$ pressure over sublimate fell to providing the required temperature difference across the section of the blank while sublimation coating.

Result and discussion. The Fig. 2.2 presents the results of forming hemispheres at a pressure of 0.4 MPa. The most uniform wall thickness in semispherical granules was achieved with a different distribution of chloride and ammonium iodide layer on the surface of the blank (see Table 2.1). Approximately the same thermal effect of sublimation coating temperature difference $T - T_c$ for ammonium chloride amounted to 100...115 °C but for ammonium iodide – total 0...50 °C, which necessitated more intense sublimation of the first sublimates and as a consequence increasing their mass.

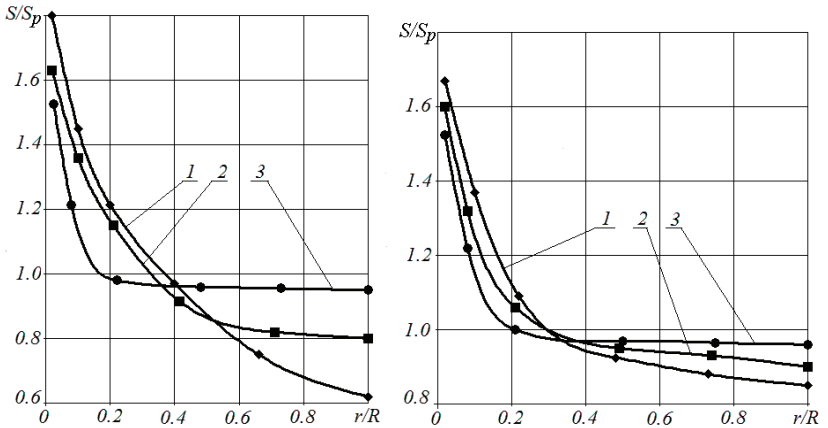

Figure 2.2. Distribution of thinning the contour of the hemispheres, formed using sublimates:
(a) 1 – isothermal SPF; 2, 3 – SPF with NH_4J and NH_4Cl coatings;
(b) 1, 2 – SPF with initiation of sublimation of NH_4Cl at $H = 0.2$ and $H = 0.3$; 3 – sublimation of NH_4Cl with the onset of SPF

Thickness variability of hemispheres on their working surfaces defined by the range $0.2 \le r/R \le 1$, was reduced by 40 … 50 %. The best result obtained for hemispheres, formed in sublimation ammonium chloride from their surface, due to the fact that in this case,

a higher temperature difference across the section of the blank at increasingly contributed to the braking strain pole shell zones.

Table 2.1. Parameters of forming hemispheres with sublimation coatings

Coating type	Beginning of sublimation	Approximating function y			ΔS , %
		A	B	Range mensuration r / R	
NH_4Cl	$H = 0$	12.5	4.0	0.32 -1.0	10
NH_4J	$H \geq 0{,}2$	12.3	4.9	0.4...1.0	16
	$H \geq 0{,}3$	12.5	5.8	0.46...1.0	26
	$H = 0$	8.9	2.7	0.3...1.0	34
Is absent	-	-	-	-	52

Analysis of graphs in Fig. 2.2a it follows that to resist deformation of the blank clamping flange hard plots has more impact than a change of temperature. In zones of flange $0 \leq r/R \leq 0.2$ variety of thickness reached 30...60 % and increased with decreasing temperature difference to be created. However, a large number of shells of the flange with the well-adjoined zones removed on subsequent operations, so the big difference of thickness on peripheral sites shells on a working surface thickness of products is not affected. If the presence of the flange in the shells on the design considerations necessarily, usually flange during operation of products designed for the perception of effort, and then it increased against the average thickness is a positive factor. For crowns with a height of 0.6 … 1.0 variety of thickness was reduced to 4...10 % on the working surface.

On Fig. 2.2b and Table 2.1 presents the results of experiments on superplastic forming of shells with sublimate. In experiments at the initial stages of forming increased pressure over the surface of ammonium chloride up to 0.6 MPa when pressure difference on both

sides of the blank 0.4 MPa. In this case the temperature of sublimation increased coverage to 470 … 480 °C and sublimation of it is absent. When the shell reached a given intermediate height, the pressure on both sides was lowered to 0.6 MPa. Thus initiated distillation coverage because its sublimation temperature at normal pressure T_c = 338 °C. Fig. 2.2b shows that there is a equable enough thinning of the shells, although the thickness of the products exceeds the similar index achieved in previous experiments. When implementing the investigated methods of SPF with thermally unstable substances, it is advisable to use equipment for molding thermoplastics with an airborne suction system, since in some cases the products of sublimation of coatings are toxic.

SPF using sublimates causes a deviation of the shell contour from a sphere-like one. This causes an inaccuracy in the calculations of the mathematical model of the SPF by the pressure of the sublimate gas. In this regard, we investigated the evolution of the shell contour in the SPF processes, which regulate the change in the thickness of the shell walls.

3. THE MATERIAL FOR PHYSICAL SIMULATION OF METAL-FORMING PROCESSES IN SUPERPLASTIC STATE

The phenomenon of super plasticity of metals (hereinafter SPM) was first observed by G. D. Bengough back in 1912, when he managed to reach elongation of a locally heated bronze sample by 160 % in a series of experiments, aimed at its slow elongation.

Up to the present time such results are still taken into account and quoted in various works [1, 18, 19]. Elongation and deformation with local heating of the blank part are applied for manufacturing shaped and elongated parts of different materials [4–13, 20-29]. Two decades later SPM ceased to be an object of exotic investigations and became an efficient foundation for creating new materials and technologies of their plastic forming, ensuring unique properties of manufactured parts and high engineering and economic efficiency of production processes [1, 14, 15, 30, 31].

Developing new technologies of super-plastic deformation presumes their simulation by application of the following ways: 1) by manufacturing industrial pilot batches [16–18, 32–34]; 2) by computer simulation [19–21, 35–37]; 3) by simulation of the processes with application of special materials [22–24, 38–40]. The first variant produces the most precise results, however it requires substantial labour consumption, that sometimes can't be justified. The second variant does not imply material expenses (except for purchasing expensive licensed computer software and training of personnel), however it largely depends upon the peculiarities of software, where a set of some or other materials models, methods of evaluation and formulae are used [25–27, 41–43]. The third variant is a simplified variant of the first variant and presumes substantial reduction of labour

consumption, due to selection of special materials for simulation, that are either relatively cheap, or they can simplify the process of simulation and raise its efficiency.

At present the second variant prevails, though computer simulation methods of deformation processes are often criticized [28, 44]. That is why the search of new modelling materials, as an alternative to the first two variants of SPM processes simulation seems to be quite vital. These material possess the following peculiarities: according to the firm opinion of many researchers [1, 29, 30, 45, 46] eutectic alloy *Sn-38%Pb*. Is the best material for simulating the processes of superplastic deformation. Selection of an alloy depends upon the following factors:

– the simplicity of forming an ultra-fine grained superplastic structure in the alloy (an intensive deformation after advisably quick recrystallization of the melt);

– high sensitivity of the flow effort to deformation rate, usually determined by the value of the coefficient of rate strengthening $t = d(ln\sigma) / d(ln\xi)$ (where σ – is flow effort, ξ – is deformation rate);

– low flow rates and high ultimate degrees of alloy's deformation;

– the range of optimal temperatures of superplasticity of *Sn-38%Pb* eutectics includes the room temperature, thus eliminating the problems with samples heating.

However, practical application of *Sn-38%Pb* alloy is connected with a series of difficulties, that are not discussed very often. In [31, 47] the fact that after intense deformation of a blank part, manufactured of *Sn-38%Pb* alloy it should be kept in a freezer, in order to avoid grain growth, occurring at the room temperature, was mentioned quite superficially (detailed explanation was missing there). Alloy deformation in optically transparent object (like, for instance, a transparent matrix at super-plastic forming) allows observing the dynamics of transformation of deformed state of the

blank). Still it is true only for the surface of the blank, if it is covered with a coordinate grid. Deformation of the inner layers of the alloy can be investigated only after the process of deformation has been completed and subsequent mechanical separation of the sample.

A perspective of application of optically transparent polymeric materials that undergo loading (deforming) with subsequent investigation of the deformed state has but lately been found. Such materials were used in experimental process, described in [32, 33, 48, 49] and in the facilities elements in [34–36, 50–52]. However, for selecting a group of materials, suitable for simulation of SPM processes it is necessary to investigate their composition and mechanical properties it has not been performed up to now.

For researchers, it is of interest to define the possibility and a degree of efficiency of application of optically transparent materials, similar to synthetic rubber for simulation of superplastic deformation.

For reaching the desired goal a material is required, having beside the advantages of *Sn-38%Pb* eutectics possesses physical and chemical properties, stable in time and at room temperature, allowing to observe deformation of both surface and internal layers of the blank, i.e. it should be optically transparent.

Block-copolymer raisins, on the basis of diene a vinyl-aroma carbons satisfy nearly all these conditions. For simulation of pressing composite in diameter cross-section samples Ø 20×30 mm in dimensions were prepared of non-linearly viscous material of polybutadiuen – 25 % polystyrene composition. On the division plane a rectangular coordinate grid was marked with Indian ink, after that the blank was placed into an optically transparent stamping facilities and a deforming load was applied.

The character of the material flow and distortion of the coordinate grid during the process of deformation was registered by a video camera during the entire process of deforming. Unlike simulation on *Sn-38%Pb* alloy, in our case, beside the data, received

by means of the coordinate grid, it was possible to build kinematic pictures of the pressing process along the flow lines, i.e. to increase the volume and the quality of the obtained data.

Simulation of other processes of plastic forming of other materials showed that it was advisable to add some quantity of polar softener and achromatic stabilizer into the block-copolymer. For that purpose a number of compositions of non-linearly viscous polymeric materials was developed for simulation of superplastic deformation, their components content is listed in Table 3.1. Block-copolymer, with achromatic stabilizers were rolled at 70 –75 ^{o}C for 2 minutes until an elastic band was formed, then a polar softener (dibutylphtalate or dibutylcebacate). Then the mixture was mixed in rolls by its partial cutting off from the rolls. The samples for testing were pressed in hydraulic press at the plates temperature 150 ^{o}C and pressure 7.5 MPa, after that they were cooled under pressure up temperature 30 ^{o}C.

Physical and mechanical tests of the samples were conducted in accordance with GOST 269, 270 for rubber materials, coefficient t was determined by the method of strains relaxation [1, 15, 30], on the samples Ø 20×30 mm in dimensions.

The results of the tests are summarized in Table 3.2.

As can be seen in Table 3.2 sensitivity of flow effort to deformation rate of the materials proposed for simulation can vary within wide limits, mostly, because of some small additions of softeners Introduction and alternation of the softerners content causes changes of strength condition of the compound, when it ubdergoes elongatoin (simplification of simulation conditions), as compared to the materials without softeners, also changed are deformation characteristics of compounds, however relative elongation value until tear remains constantly high.

Table 3.1. Composition of non-linear viscous compounds

№ №	Components	Components content, mass shares in various variants of composition													
		1	2	3	4	5	6	7	8	9	10	11	12	13	14
1	Butadienesterene block-copolymer	100	100	100	100	100	100	100	100	100	100	100	100	–	–
2	Isoprenesterene block-copolymer	–	–	–	–	–	–	–	–	–	–	–	–	100	–
3	Butadiene-α-metylsterene block-copolymer	–	–	–	–	–	–	–	–	–	–	–	–	–	100
4	2,6-di-tret-butyl-4-metylphenol	0.5	0.5	0.5	0.5	0.5	0.5	0.5	0.5	0.5	0.5	0.5	0.5	0.5	0.5
5	Dibutylphtalate	5	10	15	20	30	40	–	–	–	–	–	–	20	30
6	Dibutylsebacate	–	–	–	–	–	–	5	10	15	20	30	40	–	–

Table 3.2. Physical and mechanical properties of polymeric componds

Index	Composition variant													
	1	2	3	4	5	6	7	8	9	10	11	12	13	14
Speciifc strenth at elongation, MPa	6.5	2.9	1.12	0.45	0.31	0.14	4.17	1.82	0.84	0.38	0.20	0.1	0.19	0.42
Relative elongation until tear, %	615	502	463	268	214	145	635	560	490	312	215	167	392	309
Relative residual deformation after tear, %	18	24	52	37	26	18	22	29	56	47	32	21	41	27
Plasticity acc. to Carrer	0.29	0.51	0.59	0.64	0.72	0.90	0.34	0.54	0.63	0.70	0.77	0.92	0.68	0.60
Coeficient of rate sensitivity *t* at deformetion rates $10^{-3}...10^{-4}$ s^{-1}	0.29	0.37	0.42	0.51	0.56	1.0	0.26	0.39	0.52	0.72	1.0	1.0	0.49	0.61

Besides, changes in t parameter can be reached by selecting one or another block-copolymer. However the softener content should not exceed 40 % of the entire mass share of the block-copolymer, because: first, practically, there are no super-plastic metals and alloys with coefficient $t = 1$, and second, the material softens and poorly preserves its shape.

The compounds, registered in Table 3.1 were used for manufacturing blanks and further simulation of the metal deformation process in the state of superplasticity. A composite blank part was cast into matrix, in parts, then a rectangular coordinate grid was marked with indian ink along the cutoff plane. At simulation of the metal deformation process the prepared blanks together with the tool were placed into transparent rectangular bath, filled with water, for elimination of optical distortions, occurring as a result of changing of curvature of the surfaces of the blanks.

The conducted experiments made it also possible to build the $\sigma = f(\xi)$ diagrams in logarithmic coordinates and determine t coefficient by the tangent of inclination angle of the graphs to ξ axis (see Fig. 3.1).

The analysis of the results, summarized in Fig. 3.1 proves that just like for super-plastic metals and alloys, deformation of samples, made of block-copolymers is characterized with high rate sensitivity of the flow effort, coefficient of rate strengthening m has its maximum value within the same range of deformation rates with metallic materials. Slight changes of the softener content allows to modify either alloy's behavior with one or another super-plastic structure, or some or other temperature conditions of deforming.

Based on these exercises the following conclusions were drawn:

– simulation of the processes of super-plastic deformation with the help of optically transparent non-linear viscous block-copolymers, on the basis of diene and vinyl-aromatic carbohydrates of polar softener and achromatic stabilizer makes it possible to observe

physically the process of deformation along the entire process of samples deforming;

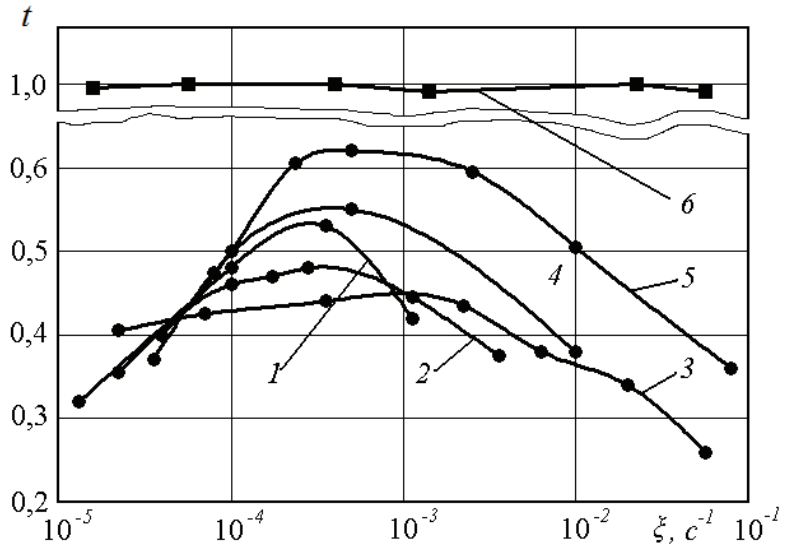

Figure 3.1. Dependence of the coefficient of rate strengthening upon rate deformation at upsetting of optically transparent block-copolymers with composition, according to Table 3.1

– by means of a coordinate grid, placed upon the diametric plane of such samples and video recording of the process it is possible to analyze quantitative and qualitative and qualitative changes along the entire volume at any time span.

4. APPLICATION OF G. LAME'S AND J. GIELIS' SUPERFORMULAS FOR DESCRIPTION OF SHELLS SUPERPLASTIC FORMING

For a control over the processes of forming, evaluating of the parameters of the deflected mode and designing of the elements of die tooling it is required to predict and describe the changing shapes of sheet blanks formed by application of SPF methods. Possibilities of new mathematical discoveries in the field of approximate description of any existing natural contours make it possible to apply Lame's [33, 34, 53, 54] and Gielis' [35, 36, 55, 56] formulas, as they seem to be very perspective. Such investigations have not been carried out yet, it ensuring scientific novelty of the work.

The processes of superplastic forming of hollow parts, manufactured of sheets (see Fig. 4.1) are calculated, as a rule, on the basis of the thin-walled moment-free (membrane) shell theory with application of Laplace's equation [1, 3, 11, 26]:

$$\frac{\sigma_1}{R_1} + \frac{\sigma_2}{R_2} = \frac{p}{S} \tag{4.1}$$

where σ_1, σ_2 – meridional and tangential stresses inside the shell at forming; R_1, R_2 – radii of the shell's curvature in the meridional and tangential directions;

As a coupling equation the equation of steady creepage is most often used [1, 3-7, 11, 26]:

$$\sigma = \omega \xi^t \tag{4.2}$$

where σ – intensity of flow stresses; ω – material's properties index; ξ – intensity of strain rates; t – strain rate hardening exponent (is an sensitivity index to evaluate the dependence of flow stress σ on strain rate ξ).

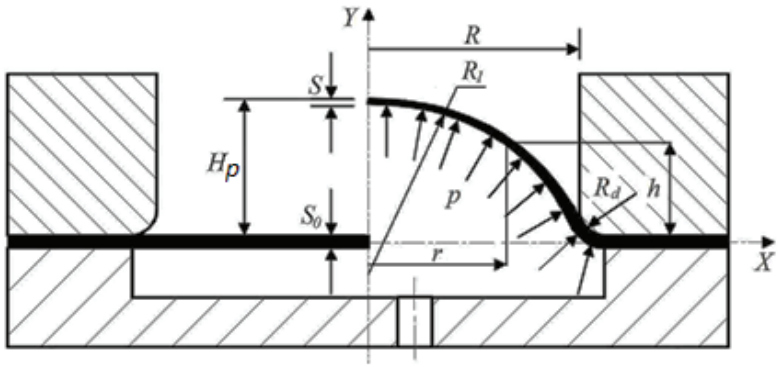

Figure 4.1. The design scheme of the superplastic forming process

At least two stages of forming [3–7] are considered for SPF calculations: 1) free bulging of the initial blank into the die-cavity to the contact with its bottom, 2) filling of angular areas of die for shells or boxes with the deformed metal. Sometimes, the forming of the triangular sections of the box-parts or the formation of rigidity ribs on the parts' surface is singled out as the third stage. The need of stage-by-stage calculation of SFP process is caused, above all, due to essential alternations of the contour's geometry of the deformed blank part at its passing from die forming to flowing into the corner areas of mating first on the bottom and side surfaces of shells and boxes and then into trihedral corners of the boxes or into the hollow parts of rigidity ribs. Besides, contact friction conditions are changed on the blank-die boundary [11, 26].

The non-monotonous evolution of the contour of a blank sheet at SPF causes drastic alternations in the radii of curvature R_1 and R_2, it complicating calculations according to Laplace's equation (4.1). The radii of curvature R_1 and R_2 are usually determined by approximating experimental data with different formulas. For the first stage of SPF it is often assumed that the contour of the formed blank is but a part of the circumference [1, 3, 11, 26], seldom it has a parabolic shape [37, 38, 57, 58] or an ellipse shape [39, 40, 59, 60]. For calculations of the corner areas parts of the contour are approximated by circumferential equations [1, 6], using polynomials and splines (equations of a chain line and circumference) [41, 61]. For evaluations of SPF technology transition from one stage to another is very often due to alternation of the system of coordinates, original assumptions, boundary conditions and the absence of interconnectivity of the indices comprising the equation (4.2). It makes the calculations more complicated, reducing their precision, it being in spite of all another prerequisite for application of Lame's and Gielis' formulas for solution of the problems of approximating the formed blanks' contours.

A number of researchers [1, 7, 38, 58] assume that the shape of blank's contour at SPF depends upon strain rate hardening exponent *t*: the bigger t-index value the closer the contour of the blank is to circumferential shape. They believe that low level of superplasticity properties of blank's metal, i.e. low values of *t*, determine transition of the contour from circle to parabolic or even hyperbolic shape [42, 62].

Still, we maintain that predicting the blank's shape at SPF, on the basis of the value of *t*-index is incorrect. The value of *t*-index is determined in connection with the entire specimen under testing. In case with SPF blanks with changed structure of separate sections and forming. In case with SPF blanks with altered structure of some sections and when forming is done within an uneven temperature field it is o normal practice to try to achieve reduced or increased

parameters of superplasticity of the deformed method inside the specified areas [43, 62]. If *t*-index is evaluated for such conditions of deformation it will be essentially less than its optimal value, according to which a geometric shape of the deformed blank is supposed to be evaluated. Due to it the contour of the crown differs from spherical shape of the sheet part, manufactured by forming [1], and the blank temperature along the crown's pole is reduced, as compared to the optimal value. According to the works [43, 62]: a) the contour of a titanium tube with a coarsened structure in the central area during superplastic expanding or flaring is closer to the bellows contour than to a circle or parabola; b) crowns (domes) during SPF of blanks with grinded grains on a some circle sector of their diameter had a contour similar to a peeled orange.

As far as SPF blanks of different thickness are concerned [13, 14, 28, 29], the crown shape at the same value of *t*-index for all sections of the blank may change both to parabolic and ellipse type. It depends on the locations of sections with maximal and minimal thickness on the blank's surface and the difference between these thicknesses in relation to the average thickness of the blank the analysis of *t*-index, described, for instance in [1, 6, 7, 16, 31] shows that its numerical values are not constant and depend on many factors, so it cannot be considered as an objective criterion for evaluating SPF parameters.

According to our opinion the conclusions of the authors of [3, 7, 37, 45, 57, 64] works seem to be relevant, when they ascertain that the shape of the contour (profile) of a deformed blank part depends on distribution of its relative thickness. It can be explained by the following reasons:

1) it was found experimentally [1, 3, 7, 44-45, 64, 65], that for smith SPF the maximum deviation of the crown's shape from spherical shape was observed at the smallest values of S/S_0 in the crown's pole;

2) prior to fracturing of the crown's walls, a local bulging of the crown with abnormal decrease in the radius of curvature takes place, simultaneously with a drastic decrease of the blank's thickness, this phenomenon is typical to both superplastic and ordinary cold forming of parts, like, for instance, by liquid pressing [2, 3];

3) adjusting the blank's thinning (as a rule, reduction of difference in thicknesses of its walls) by SPF methods of variable thickness, by preliminary preparation of different structures in the specified sections and in an even temperature field is accompanied with an evident deviation of the crown at the stage of smith forming, from the shape of spheroid segment [1, 8, 13, 14, 28-30, 43, 62].

The performed review shows the vitality of finding ways of approximation of contours of sheet blanks at superplastic forming, by application of a unified equation, for the sake of unifying the approaches to a detailed analysis of shape alternation and tools' contours design in order to ensure their standard durability.

For selection of a universal equation for description of shells' contours, formed under conditions of superplasticity it should be noted that its diagrams must describe different shapes of parabolas, circumferences, and rectangles with rounded angles, at different values of parameters, comprising it.

We assume that such equations may comprise an equation of Gabriel Lame's curve, more widely known as a "superellipse" [33-34, 53, 54], and Johan Gielis' equation [35, 36, 55, 56], known also a "superformula".

The "superellipse" is generally described in Cartesian coordinated with the following equation:

$$\left(\frac{x}{a_0}\right)^n + \left(\frac{y}{b_0}\right)^m = 1 \tag{4.3}$$

where n and m – exponents; a_0 and b_0 – coefficients, $a_0 > 0$, $b_0 > 0$.

Depending on the values of n, m, a_0 and b_0 diagrams of the equation (4.3) describe the entire set of contours, that sheet blanks may have at different SPF stages.

Johan Gielis offered in his classical work [35, 55] a more generalized equation, known nowadays a "superformula", it may be applied for describing many complicated shapes and curves, that are met in nature and engineering [36, 56]. In geometrically opposite coordinates for radius-vector r^V and φ angle the equation has the following view:

$$r^V = \left\{ \sqrt[n_1]{\left[\left|\frac{1}{a_1}\cos\left(\frac{k}{4}\varphi\right)\right|\right]^{n_2} + \left[\left|\frac{1}{b_1}\sin\left(\frac{k}{4}\varphi\right)\right|\right]^{n_3}} \right\}^{-1} \qquad (4.4)$$

where n_1, n_2, n_3 – curve's shape indices; a_1, b_1 – dimensions (values of semi-axes); k – index of the number of repeated fragments.

The authors rightfully consider the equation (4.4) to be a new way of describing and represented natural objects and maintain that the variety of shapes can be described with one singular and simple numeric equation. The circumferential equation, reduced to more general view and having acquired the view of (4.4) equation can form lots of generations of different curves and polygons, including shells' contours at SPF.

Now, let us consider the graphs of the "superformula" (4.4), its parameters n and m are changed within 1-24 limits (see Fig. 4.2). Lame's superellipse (4.3) is its particular case ($n_1 = n_2 = n_3 = 4$) and it represents a rectangle with rounded angles. As the sought values at shells SPF are normally investigated in non-dimensional parameters (with regard to the highest values of the initial blank's thickness S_0, the radius of the shell's base R, the final height of the shell H_p, etc.) of interest to us, first and foremost, there will be graph's sections within $0 \le x \le 1$ and $0 \le y \le 1$ intervals. To do it we'll assume $x = X = r/R$, $y = Y = h/R$, $a_1 = R_1/R = 1$, $b_1 = H_p/R$. The graphs, situated in the first

quadrant of the coordinate plane may be expressed in other quadrants symmetrically with regard to the coordinate axes.

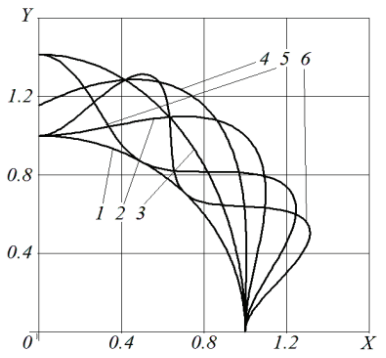

(a)

(a): 1 – $k = 4$, $n_1 = n_2 = n_3 = 2$;
2 – $k = 4$, $n_1 = n_2 = 4$, $n_3 = 2$;
3 – $k = 2$, $n_1 = n_2 = 4$, $n_3 = 2$;
4 – $k = 3$, $n_1 = n_2 = 4$, $n_3 = 2$;
5 – $k = 6$, $n_1 = n_2 = 4$, $n_3 = 2$;
6 – $k = 8$, $n_1 = n_2 = 4$, $n_3 = 2$

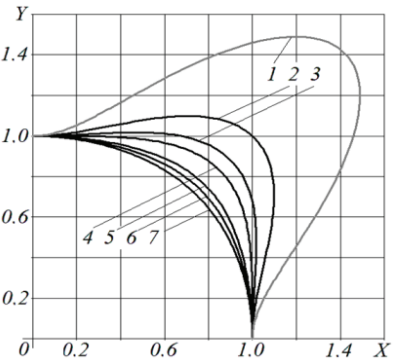

(b)

(b): 1 – $k = n_1 = n_2 = 4$, $n_3 = 1$;
2 – $k = n_1 = n_2 = 4$, $n_3 = 2$;
3 – $k = n_1 = n_2 = 4$, $n_3 = 3$;
4 – $k = n_1 = n_2 = 4$, $n_3 = 4$;
5 – $k = n_1 = n_2 = 4$, $n_3 = 8$;
6 – $k = n_1 = n_2 = 4$, $n_3 = 12$;
7 – $k = n_1 = n_2 = 4$, $n_3 = 24$

Figure 4.2. Superformula graphs at $a_0 = b_0 = 1$ and different values of n_1, n_2, n_3, k parameters

Fig. 4.2 shows what additional possibilities can be revealed in Gielis' superformula in comparison with Lame's superellipse by introducing into it $k/4$ multiplier. Only curve 1 which parameters $n_1...n_3$ characterize it as a circle at $k/4 = 1$ or $k = 4$ is inscribed in the coordinate area restricted by $0 \le x \le 1$ and $0 \le y \le 1$ boundaries. In other cases superformula's graphs exceed the above-mentioned bounds, showing their periodicity, typical of trigonometric equations, which comprise the superformula. With regard to symmetry of graphs

on relation to the coordinate axes, the number of periods in the first quadrant of Cartesian coordinates is determined by the value of $k/4$. At $k/4 = 2$ (the same $k = 8$) there will be 2 (see Fig. 4.2, 6 curve) at $k/4 = 1{,}5$ or $k = 6$ and one period and a half (curve 5), etc.

Thus, introduction of the parameter of $k/4$ into the equation (4.4) allows overcoming the main disadvantage of "superellipses" – their limitations in symmetry. If k – parameter is available the plane may be divided into a multitude of sectors, their number is equal to k instead of four quadrants in Euclidean plane. For example, at $k = 3, 4, 5 – N$ is curve which described in four quadrants by means of equation (4.4) will have 3, 4, 5 – N number of repeated fragments.

The higher the level of symmetry of analyzed contours the simpler view the superformula (4.4) acquires, as the indices $n_1 ... n_3$, and in some cases the values of a_0 and b_0 semi-axes become equal to each other. Because of it, bearing in mind the objective of our work, the multiplier $k/4 = 1$or $k = 4$ should have been used in the superformula.

Fig. 4.2b represents the evolution of graphs of the superformula at different values of n_3 parameter. An essential change in the curvature of graphs 1 – 3 and their retreat from the beginning of the coordinates at $n_3 < 4$ is the reason for their unfitness for approximation of shells' contours at SPF. If $n_3 \geq 4$, then graphs' appearance is qualitatively changed, same as at similar changes at n and m in Lame's superellipse, in condition that $n = m$.

Thus, if approximation of most common shells' contours formed in the superplastic state from sheets is the case, when one or several planes of symmetry are present (spheres, cylindrical shells, round and square boxes) both equations (4.1) and (4.4) are applicable. The approximation by Lame's superellipse seems to be easier, as it requires determination of numerical values of two coefficients n and m only. More intricate shells' contours (boxes equipped with rigidity

ribs, cylindrical shells with undercuts, pieces, having surfaces with different curvature radii, etc.) should be approximated by Gielis' "superformula".

Discussion and application. Now, let us analyze the possibilities of describing shells' contours by means of Lame's superellipses (see Fig. 4.3).

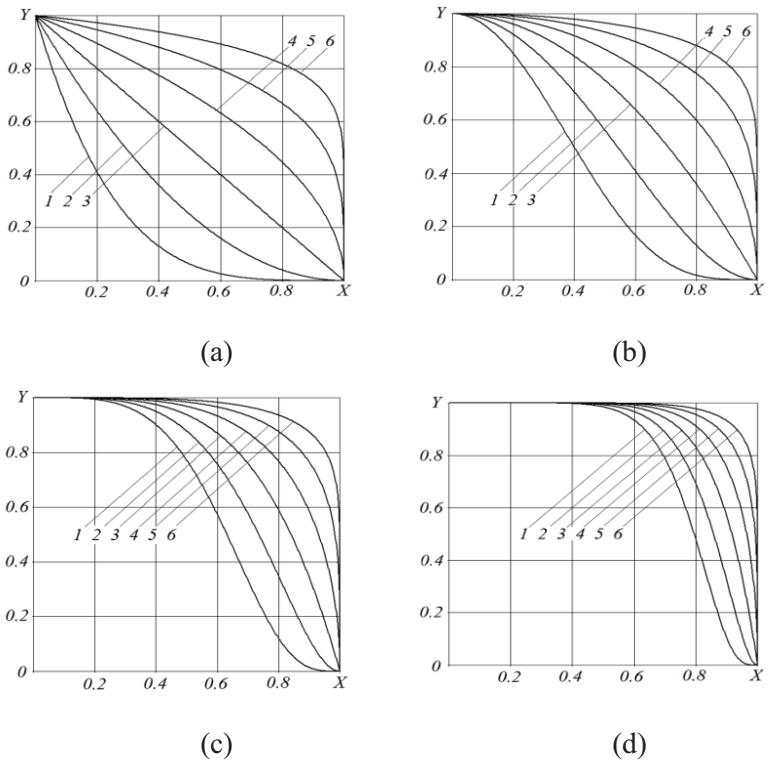

Figure 4.3. Graphs of "superellipses" at $a_0 = b_0 = 1$ and different values of n and m parameters:
(**a**) – $n = 1$; (**b**) – $n = 2$; (**c**) – $n = 4$; (**d**) – $n = 8$; **1** – $m = 0.25$; **2** – $m = 0.5$; **3** – $m = 1$; **4** – $m = 2$; **5** – $m = 4$; **6** – $m = 8$

The analysis of the graphs shows that the equation (4.3), in which $n \leq 1$ at all values of m from 0.25...8 interval are inapplicable for approximation. Even at $m = 4$ and $m = 8$ the graphs (Fig. 4.3a) in the point with $x = 0$, $y = 1$ coordinates have the inclination angle to x axis, not equal to zero, it being impossible both in case of crowns formation and for SPF of shells and boxes. The curves of the equation (4.3) (see Fig. 4.3b) at $n = 2$ and $m \geq 1$ could be, in principle applied for approximation of both parabolic and ellipse-like contours of shells at the first SPF stage and also for description of formed contours and shells at the second stage of SPF.

The graphs of the "superellipses" in Fig. 4.3c at $n = 4$ can be used approximation of several variants of shells' contours. At $m \geq 1$ values graphs 3 - 6 simulate the contour of the shells, the crown of which has reached the die bottom and the second SPF stage has begun. At $n = m = 4$ the angular areas are formed with equal strain of the polar and flange areas of the shells, at $m = 1$ and 2 it happens with prevailing of thin polar areas, at $m = 8$ – at deceleration of shell's deformation in the polar areas by when frictional forces rub against the die and the shell's angular areas are formed mainly by means of thinning blank's section, located near the flanges.

The curves 1 and 2 ($m = 0.25$ and 0.5) in the point with $x = 1$, $y = 0$ coordinates have some overbending, it allowing their application for approximation of shells' contours with due regard to the radius of rounding of the die.

It is shown in Fig. 4.3d that by applying of the superellipse at $n = 8$ it is possible to simulate the contour of shells, forming angular areas, mainly, due to deformation of the central sections of the shell. At $n = m = 8$ deformation of the polar and flange areas of the shell is nearly the same, while the radius of rounding of the angular area is essentially less, than for the curve with $n = m = 4$. Curves 1 and 2 ($m = 0.25$ and 0.5) have an overbending in the point with $x = 1$, $y = 0$

coordinates, just like Fig. 4.3c, although their radius is smaller so they can express the shells' contour with and without the rounding radius of the die.

The advantage of the analyzed equation is its possibility to determine by means of the value of coefficients, described above, the contour of the manufactured part and, hence, the stage of SPF, which the "superformula" describes, as well as the presence of superplasticity properties of deformed metal. In mathematics a parameter of rectangularity $\eta = 2/n$ (here is $n = m$) is introduced for these purposes. The closer to one the value of η is, the closer to circumferential shape the contour of the deformed part is at the stage of blow molding, i.e. the bigger is the level of superplasticity properties of deformed metal.

The values $2 > \eta > 1$ testify a low level of blank's metal superplasticity, and transition of its spherical contour (in the first two quadrants of the crossing plane, i.e. at positive ordinates) into parabolic and then up to conical (at $\eta = 2$ and $n = m = 1$), that can take place at filling of rigidity ribs with a triangular contour in section. In all four quadrtants the graph of the superformula has a shape of a rhombus, rectangle or a square with vertices on the coordinate axes.

At $4 > \eta > 2$ ($n < 1$ and $m < 1$) the superformula is gradually transformed into an astroid ($\eta = 4$). The values of n and m smaller than one testify errors, occurred, while approximating with the superformula.

The interval of $2 < (n, m) < 4$ or $1 > \eta > 0.5$ values gives us an opportunity to assume that the process of SPF is carried out with deceleration of deformation of the central areas of the blank. The contour of the blank is rearranged from spherical to elliptic. At $n = m = 4$ (the variant of the superformula is "superellipse" thoroughly investigated by Lame) the curve's contour acquires a rectangular shape with quite an essential radius of sides coupling in the angles. It can be maintained that the superformula describes in this

form the second stage of SPF – filling of the angular zones of cylindrical or box-shaped parts. The radius acceptable for parts of shell or box type in angles, equal to two-four thicknesses of the blank is reached at (n and m) = 7...10.

Besides, if $n > m > 4$, then at the second stage of SPF deformation of the crown's central areas occurs, exceeding deformation in the blank's sections, close to flanges. It may occur if there is some efficient lubricant with low constant of friction between the bottom of the die and central areas of the crown. The shape of the semi-finished product is characterized by presence of flat polar surface, transferring into parabolic or hyperbolic surface of peripheral sections, which have no contacts with the side surface of the die.

The superformula with $m > n > 4$ is applicable if the blank before the SPF was subjected to a deep drawing by rigid punch (pneumomechanical forming). The graph of the superformula has a straight vertical section near the flange passing into an elliptical curve that ending in the pole of the crown.

Now, let us consider shells' geometrical shape at two stages of SPF: (a) – at $H_p = R$ (at the first stage and (b) – at $H_p = 0{,}6R$ (the next stage). We'll also consider the peculiarities of its approximation by Lame's equation, using the data listed in [38, 46]. As was mentioned before, the choice of the is explained by the presence of a big number of axes and planes, due to which application of more complicated Gielis' formula is hardly advisable.

For approximations of contours at $H_p = R$, the shells manufactured of *AlMg5* and *Sn-38%Pb* alloy were chosen with different values of *t*-index, and of *AlMg6* [38, 46, 58, 66] alloy also. Blanks, made of *AlMg6* alloy had a variable thickness: $S_0 = 1.45$ mm in the central part with a diameter of 60 mm, and $S_0 = 1.23$ mm in a ring peripheral section with outside and inside diameters being of 100 and 60 mm, respectively.

For approximation of contours at $H_p = 0{,}6R$, the shells manufactured of *AlMg3* [46, 66] alloy were chosen, having the shape of: a) spherical-like segments, formed at the first SPF stage under isothermal conditions and in uneven temperature field; b) intermediate semi-finished shells, formed at the second SPF stage into a cylindrical die.

Table 4.1 represents Lame's equations (after the transformations and simplifications) for approximating shells' contours at $H_p = R$ and $H_p = 0{,}6R$.

Because many researchers [1–3, 43, 62] presume that a contour of a shell of small height at the initial stages of SPF has a shape of spherical segment, it is expedient for further analysis of such assumption to define more exactly the types of equations of Lame's superellipse for these cases.

The spherical segment formed at initial stages of blank's bulging has the contour approximated by circumferential equation:

$$\left(\frac{x}{R_k}\right)^2 + \left(\frac{y}{R_k}\right)^2 = 1 \tag{4.5}$$

where R_k – is the radius of the circumferential curvature, forming segment's contour with $2R$ chord and H_p height.

The radius R_k of curvature is related to the current height h and the radius R of segment's base (cap) by following ratio:

$$R_k = \frac{R^2 + h^2}{2h} \tag{4.6}$$

Designating $h = \beta R$, we can write down the equation (4.5) in this view:

$$\left[\frac{2\beta x}{(1+\beta^2)R}\right]^2 + \left[\frac{2\beta x}{(1+\beta^2)R}\right]^2 = 1 \tag{4.7}$$

Table 4.1. The equations of approximating of actual shells' contours at SPF

For shells with $H_p = R$		For shells with $H_p = 0{,}6R$	
Shell's parameters	Approximating equation in dimensionless view	Shell's parameters	Approximating equation in dimensionless view
AlMg6 alloy, blank of variable thickness	$Y_{AlMg6} = \left(1 - X_R^{2.58}\right)^{0.51}$ (Y_2)	SPF of the segment in uneven temperature field	$Y_{TF} = 0.6\left(1 - X_{TF}^{2.36}\right)^{0.813}$ (Y_1)
Sn-38%Pb alloy, $t = 0.6$	$Y_{t0.6} = \left(1 - X_R^{2.02}\right)^{0.521}$ (Y_3)	Forming with shell's lubrication	$Y_L = 0.6\left(1 - X_L^{3.03}\right)^{0.756}$ (Y_6)
Sn-38%Pb alloy, $t = 0{,}25$	$Y_{t0.25} = \left(1 - X_R^{1.98}\right)^{0.581}$ (Y_4)	Forming without shell's lubrication	$Y_{NL} = 0.6\left(1 - X_{NL}^{2.58}\right)^{0.61}$ (Y_7)
AlMg5 alloy	$Y_{AlMg5} = \left(1 - X_R^{1.99}\right)^{0.562}$ (Y_5)	Segment's SPF in isothermal conditions	$Y_P = 0.6\left(1 - X_P^{1.94}\right)^{0.781}$ (Y_8)

Let us transfer the beginning of coordinates for (4.7) equation to the point of intersection of height and base radius of the segment, i.e. at a distance along *y*-axis, equal to $(R_k - h)$, then, the equation (4.7) will acquire the following view:

$$y = h\left(\frac{1+\beta^2}{2\beta}\right)\left\{1 - \left[\frac{2\beta x}{(1+\beta^2)R}\right]^2\right\}^{1/2} - h\left(\frac{1-\beta^2}{2\beta}\right) \qquad (4.8)$$

or in dimensionless view:

$$Y_{SG} = \left(\frac{1+\beta^2}{2\beta}\right)\left\{1 - \left[\frac{2\beta X_{SG}}{(1+\beta^2)}\right]^2\right\}^{1/2} - \left(\frac{1-\beta^2}{2\beta}\right) \qquad (4.9)$$

Particularly for semi-spherical shell ($\beta = 1$, $R_k = h = R$) we'll have:

$$y = R\left[1 - \left(\frac{x}{R}\right)^2\right]^{1/2} \quad \text{or} \quad Y_0 = (1 - X_0^2)^{1/2} \qquad (4.10)$$

where $Y_0 = h/R$, $X_0 = h/R$ – are dimensionless coordinates of circumferential contour's points, changing within $0 \leq (r, h) \leq 1$ interval.

Relative deviations q of real contours of shells with $H_p = R$ and $H_p = 0{,}6R$ from semi-spheres' contours Y_0 and spherical segments Y_{SG} with the radius of the base (cap) R are presented in Fig. 4.4 and Fig. 4.5. The relative deviation was determined as $q = Y_i/Yj$, where Y_i – are approximating functions of real contours of shells (see Table 4.1); Y_j – circumferential equations Y_0 (4.10) and equations of the spherical segment Y_{SG} (4.9).

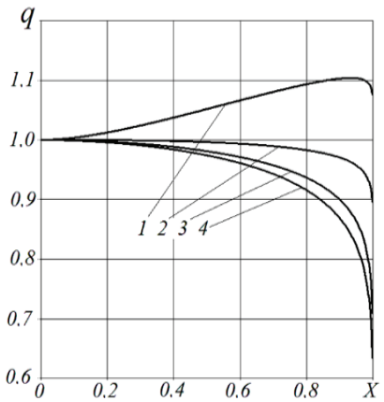

Figure 4.4. Distribution of the relation of ordinates of shells' contours at $H_p = R$ and a semi-sphere along the radius of base (cap):

1 – $q = Y_{AlMg6}/Y_0$;
2 – $q = Y_{t0.6}/Y_0$;
3 – $q = Y_{AlMg5}/Y_0$;
4 – $q = Y_{t0.25}/Y_0$

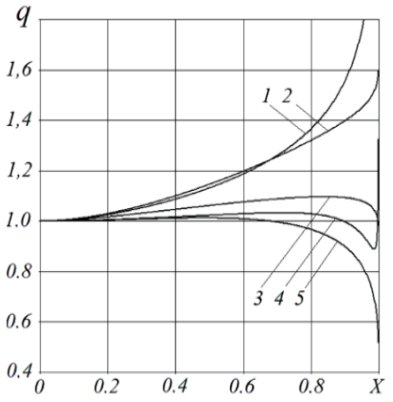

Figure 4.5. Distribution of the relation of ordinates of shells' contours at $H_p = 0.6R$, made of *AlMg3* alloy along the radius of base (cap):

1 – $q = Y_{NL}/Y_P$;
2 – $q = Y_L/Y_P$;
3 – $q = Y_{TF}/Y_P$;
4 – $q = Y_0/Y_P$;
5 – $q = Y_L/Y_{NL}$;

All equations do not take into account the presence of the radius R_d of conjugation of deformable shell and the flange, i.e. they are not true within $r = (0{,}95 \ldots 1{,}0)R$ interval.

Curves 2 – 4 in Fig. 4.4 confirm the data of researchers [38, 42, 46, 58, 62, 66] that the contour of the shells molded free in the die-cavity is determined by the level of superplasticity properties of material. The smaller it is (small t-index value, greater multi-thickness of shells') the bigger is the deviation of the contour from spherical shape towards parabola. At that in the equations of approximation we have $m < n < 2$. However, if a blank of variable thickness is used for the SPF, the resulting change in the stress state will cause the

displacing of the shell contour in central zones at the initial stage of the SPF toward the ellipse view (curve 1, Fig. 4.4). The approximation function Y_{AlMg6} is characterized here by $n > 2$ index, while $m < 2$, it being possibly caused by low of superplasticity properties of *AlMg6* alloy.

As can be seen from the graphs in Fig. 4.5, parabolic shape of shell also occurs at its lower height $H_p = 0{,}6R$ (curve 4). Deviation q does not exceed 0.03 here within a reliable interval of change, while for shells with $H_p = R$ the q-parameter is within 0.04...0.18 intervals.

The chilling of a blank by water droplets falling from hodograph at 20 seconds interval upon the polar areas ensured uneven temperature field along the shell's contour at its forming during the initial stage of SPF. As a result of deceleration of thinning of central shells' areas, its contour within the areas of the pole deviated from spherical shape towards ellipse, just like in case with application of a blank with variable thickness (see curve 3, Fig.4.5). The maximum ratio of the ordinates of the approximating equation Y_{TF} and Y_p was $q_{max} = 1.1$ at $X = 0.84$.

Because of chilling of the central surface of the deformed blank it was not possible to mold the high crowns. Breakage of crown's walls was registered not in the pole, but in sections of the surface between the pole and the flange, and walls thickness in the polar areas was approximately equal to the thickness of walls in sections where metal breakage was observed.

The second stage of SPF at forming of a cylindrical shell with $H = 0.6R$ produces a contour of semi-finished product essentially dependant on presence of lubrication on the bottom surface of the die changing the character of metal flow at filling of the shells' angles.

At forming without lubrication the shell's sections which are in contact with the bottom of die are not deformed nearly and shell's contours are formed due to thinning of free zones of the shell. Presence of lubrication of "shell-bottom" boundary causes further thinning of polar areas at the second stage of SPF [6, 46, 66]. The contour of semi-

finished product acquires a straight area originating in the pole of the crown and eventually passing to a parabolic curve propagating along the radius of conjugation of the die into the blank's flange. The straight area of the contour eventually grows bigger (the radius of shell's curvature increases) while such straight section of the contour appears later. The shell's ordinates in these areas are increased in direction of the bottom of the die with higher intensity, as compared to forming without lubricating (see curves 1 and 2, Fig. 4.5). Meanwhile, deformation of the areas near flanges is more intense at forming without lubrication. The curve 5 (Fig. 4.5) shows that within $0 < r/R < 0.68$ interval the ordinates of shell's semi-finished product are higher at SPF with lubrication, while the opposite state can be seen at areas near flanges.

5. ANALYSIS OF THE SHEET SHELL'S CURVATURE WITH LAME'S SUPERELLIPSE METHOD DURING SUPERPLASTIC FORMING

The performed research shows the vitality of finding ways of approximation of contours of sheet blanks at superplastic forming, by application of a unified equation, for the sake of unifying the approaches to a detailed analysis of shape alternation and tools' contours design. The study of the distribution of the radii of curvature R_1 and R_2 of shells at the stages of free SPF and the formation of angular zones is an actual task necessary for the development of ways to control the geometry and properties of shaped articles such as cylindrical boxes. The formula Lame is considered by us as a new, very simple and universal mathematical tool, which until now has not been used to solve such important problems as the description of the curvature elements of formable shells.

The values of the principal radii of curvature of the shells $R_{1p} = R_1/R$, $R_{2p} = R_2/R$ in dimensionless coordinates can be calculated from formulas

$$R_{1p} = \{1 + [y'(x)]^2\}^{3/2} [y''(x)]^{-1}; \qquad R_{2p} = -y(x)\{1 + [y'(x)]^2\}^{1/2} \tag{5.1}$$

If we use the Lame formula as a function $y = f(x)$, then

$$R_{1p} = \frac{\left[1+(b_0 n/m)^2 a_0^{-2n/m} x^{2(n-1)} (a_0^n - x^n)^{2(1-m)/m}\right]^{3/2}}{-(b_0 n/m) a_0^{-n/m} x^{n-2} (a_0^n - x^n)^{(1-2m)/m} \{(n-1)(a_0^n - x^n) + [(m-1)/m] n x^n\}} \tag{5.2}$$

$$R_{2p}=-b_0 a_0^{-n/m}(a_0^n-x^n)^{1/m}\left[1+(b_0 n/m)^2 a_0^{-2n/m}x^{2(n-1)}(a_0^n-x^n)^{(2-2m)/m}\right]^{1/2} \quad (5.3)$$

Quite often in equation (4.3) we can take $n = m$, then

$$R_{1p}=\frac{a_0^{1-n}x^{2-n}(a_0^n-x^n)^{(2-1/n)}\left[1+\left(b_0/a_0\right)^2 x^{2(n-1)}(a^n-x^n)^{(2/n-2)}\right]^{3/2}}{b_0(1-n)} \quad (5.4)$$

$$R_{2p}=-\frac{b_0}{a_0}(a_0^n-x^n)^{1/n}\left[1+\left(\frac{b_0}{a_0}\right)^2 x^{2(n-1)}(a_0^n-x^n)^{(2/n-2)}\right]^{1/2} \quad (5.5)$$

If the Lame formula is written in parametric form, ie

$$x = r_\alpha \cos^{2/n}\alpha,\ \ y = h_\alpha \sin^{2/m}\alpha, \quad (5.6)$$

where $r_\alpha = r/R$, $h_\alpha = h/H_p$), then the meridional radius of curvature can be calculated by the formulas:

$$R_{1p}=\frac{\left(\frac{4r^2}{n^2}sin^2\alpha\, cos^{(4/n-2)}\alpha+\frac{4h^2}{m^2}sin^{(4/m-2)}\alpha\, cos^2\alpha\right)^{3/2}}{-\frac{4rh}{nm}sin^{(2/m-1)}\alpha\, cos^{(2/n-1)}\alpha\left[\left(\frac{2}{m}-2\right)cos^2\alpha+\left(\frac{2}{n}-2\right)sin^2\alpha\right]} \quad (5.7)$$

or (at $n = m$):

$$R_{1p}=\frac{\left(\frac{4r^2}{n^2}sin^2\alpha\, cos^{(4/n-2)}\alpha+\frac{4h^2}{m^2}sin^{(4/m-2)}\alpha\, cos^2\alpha\right)^{3/2}}{-\frac{4rh}{n}\left(\frac{2}{n}-2\right)sin^{(2/m-1)}\alpha\, cos^{(2/n-1)}\alpha} \quad (5.8)$$

In Fig. 5.1 shows the changes in the principal radii of curvature R_{1p} and R_{2p} of the shell contours along their base radius. For $R_{1p} = R_{2p} = -1$, the shell contour is perfectly spherical, and the sign "-" means that their centers are below the shell contour.

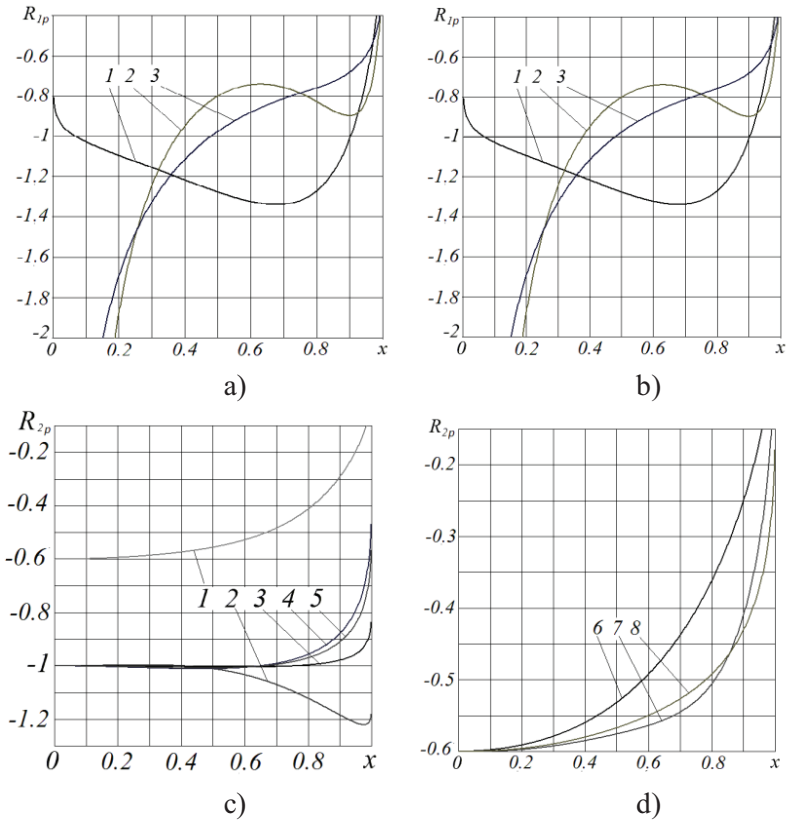

Figure 5.1. Distribution of the values of the main radii of curvature R_{1p} and R_{2p} along the radius of the shell base in the SPF:
a, b – free forming of segments with relative height $y = 1$ and 0.6;
1 – 5 – respectively for contours $Y_{1...5} = f(x)$;
c, d – forming a cylindrical beaker with $y = 0.6$;
1 – 3 – respectively for the contours $Y_{6...8} = f(x)$ (see Table 4.1)

The hemisphere from *Sn-38% Pb* alloy with a high coefficient $t = 0.6$ is characterized by a sufficiently uneven meridional radius R_{1p} deviating from $R_{1p} = -1$ by no more than ± 5 %. A slightly larger spread of R_{1p} (± 15 %) is fixed for the hemisphere from the *AlMg5* alloy. In shells from babbit with $t = 0.25$ deviations of R_{1p} from unity are more significant: (- 15 ÷ + 45) %.

The regulation of refinement of the blank in the SPF leads to huge values of R_{1p} in the zone of the shell pole ($x = 0...0.1$), that is, to the presence of practically horizontal areas. For hemispheres from blanks of variable thickness, a minimum of R_{1p} is fixed in the areas of linking the thick and thin parts of the blanks ($R_{1p\ min} = -0.76$ at $x = 0.57$). For segments with $y = 0.6$ formed in an uneven temperature field, the cooling of the pole does not extend to the whole deformable surface, so the deviation of the radius R_{1p} from -1 in the range $x = 0.17...0.95$ does not exceed ± 20 %.

The tangential radius of curvature R_{2p} for hemispheres made of the *AlMg5* and *Sn-38% Pb* alloys decreases monotonically from $R_{2p} = -1$ only at $x > 0.65$. The intensity of decline is higher, the lower the level of superplastic properties of the blank material.

The hemisphere 2 for $x = \leq 0.5$ is characterized by the equality $|R_{2p}| = y \sim 1$, in sections with $x > 0.5$, the smaller thickness of the blank (1.23 mm) causes an increase in $|R_{2p}|$ in 1.2 times.

The SPF in an uneven temperature field with $y = 0.6$ causes a contour with a constantly decreasing value $|R_{2p}|$ from the pole to the flange, at that the difference in the values of R_{2p} for $x = 0$ and 0.95 is 4...8 times higher than for babbitt shells with a coefficient of $t = 0.25$ and 0.60.

Free forming of the dome with a height of $y = 0.6$ provides values of the radius R_{1p} in the interval ($x = 0...0.95$) from $R_{1p} = -0.8 \div -0.7$ to $R_{1p} = -1.34$ at $x = 0.68$. The second stage of forming a cylindrical beaker is characterized by abnormally high values of R_{1p} in the poles of the zones of the formed semi-finished product. When the beaker is formed without lubrication, the values of

R_{1p} of its contour decrease in the direction from the pole to the flange, and at $x \sim 0.7...0.8$ the curve of $R_{1p} = f(x)$ takes place. Presence of lubrication between the matrix and the formed semi-finished product causes a more intensive decrease of R_{1p} to a minimum of $R_{1p\,min} = -0.74$ at $x = 0.63$ and the subsequent growth of R_{1p} to $R_{1p\,max} = -0.9$ at $x = 0.9$. Thus, in the range $x \sim 0.25...0.7$, the presence of lubricant reduces R_{1p} with the SPF angles of the beakers.

For all SPF stages of cylindrical beakers, the tangential radius of curvature R_{2p} in the pole is equal to the absolute value of the height $y = 0.6$ and decreases monotonically to the flange zones. However, in comparison with the SPF of the spherical segment, the design of the contour of the bottom of the beaker is accompanied by a decrease in the intensity of the change in R_{2p} by a factor of 2...3. In the interval ($x = 0...0.86$, $R_{2p} = -0.6…-0.46$), the radius R_{2p} decreases at the SPF to a lesser extent with the presence of a lubricant, which indicates a more uniform plastic flow of the metal.

Fig. 5.2 shows the dependence of the meridional radius of curvature R_{1p} from the angle of its inclination α to the x-axis with the vertex in the center of reference of the radius vector R_{1p}. The graphs of the function $R_{1p} = f(\alpha)$, calculated by formula (5.7), clearly show that for any variants of the contours that form the angles of the shells in SPF, the radius R_{1p} will be a variable, and the center of its reference in the general case will not be on the bisector of the angle between the bottom and walls of the glass.

SPF of the corners of the cylindrical shell in the presence of oil (curves 1, 3, 4) can provide a minimum of R_{1p} on the contour section, which is located either closer to the wall of the matrix, or, in some cases, on the bisector.

The absence of oil between the bottom of the matrix and the shell causes a minimum of R_{1p} in the area of the contour (curve 2), which is distant from the bisector in the direction of the bottom of the matrix. The reference centers of radii R_{1p} in all cases under consideration are shifted in one direction or another from the bisector.

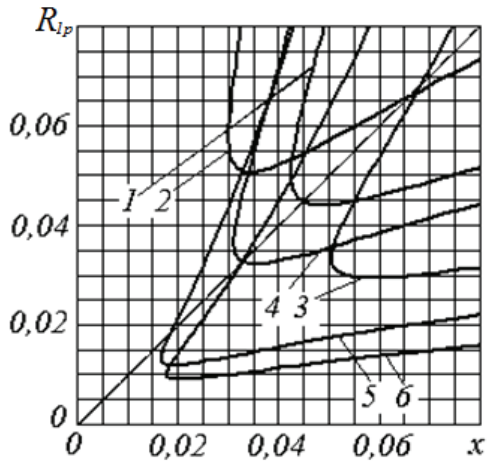

Figure 5.2. Graphs of the dependence of the meridional radius of curvature R_{1p} on the angle of its inclination α to the x-axis at the SPF of the angular zones of the glasses having contours for which:
1 – n = 23.6, m = 13.2; 2 – n = 32, m = 9; 3 – n = 15, m = 19;
4 – n = 32, m = 18; 5 – n = 50, m = 50; 6 – n = 36, m = 60

The calculated graphs of the contours of the shells with smaller radii R_{1p} are presented on curves 5, 6 and show qualitatively the same results. The differences are that the growth of R_{1p} in both directions of change of the angle α is different in intensity and absolute values.

If in the second stage of the SPF there is no oil between the workpiece and the stamp, then at the same pressure P and the formation time τ the minimum R_{1p} will be greater than in the SPF with the oil. It is possible to achieve the same minimum radius R_{1p} by increasing the force P or time τ as when using the oil, but this minimum will be closer to the wall of the glass, and its growth in both directions is slower (curve 3).

As a special case, it may happen that in the corner zones of the shell at least R_{1p} will be equidistant from the bottom and walls (curves 1, 4). The contours of cylindrical shells with a reduced radius R_{1p} are

characterized by an approximating function (5.3) with larger values of the coefficients n and m (curve 4). If $n \le m$, then the minimum R_{1p} should always be closer to the walls of the glass, but due to the rigid pressure of the workpiece flange to achieve a minimum in the area of contact of the workpiece with the wall and not with the bottom of the matrix, according to our data, impossible.

Consider SPF of angles, for example, beakers with dimensions of Ø 200×60 mm ($y = 0.6$) in the matrix with an angle of 90° between the bottom and the walls. In Fig. 5.3 shows the contours of the angular zones of the beakers for various SPF variants. The parameters of the contours for these zones are given in Table 5.1.

For plotting curves 4 - 6, the centers of the radii R_{1p}^{x} and R_{1p}^{y} were determined on the normals to curves 1 - 3 at the corresponding points with coordinates X, Y. The normals were calculated by the formula:

$$h\left(\frac{r^n - x^m}{r^n}\right)^{1/m} - Y = (x - X)\frac{m}{nh} r^{n/m} x^{1-n} (r^n - x^n)^{1-\frac{1}{m}} \qquad (5.9)$$

For a really achievable contour $1 - R_{1p}{}^{min} = 0.063$ and $r^{min} = r \cdot R_{1p} = 6.3$ mm. The mutually perpendicular distances from the radius reference center to the contours in the bottom and the wall of the matrix are respectively $R'_{1p} = 6.5$ and $R''_{1p} = 6.6$ mm, respectively, that is 3...5 % more than R_{1p}^{min}. The radiuses of curvature in these places are respectively $R''_{1p} = 16.7$ and $R'_{1p} = 16.8$ mm that is, 2.65 times greater than R_{1p}^{min}. The centers of these radii $R_{1p}^{y}$and R_{1p}^{x} are located on the parabolic curve 4, which is separated from the bisector 7 of the angle between the walls and the bottom of the matrix, respectively, in the sides of the wall and the bottom of the matrix. The larger the change in the radius R_{1p} in the sections of the contours in

question, the more intense the deviation of the parabola from the bisector 7.

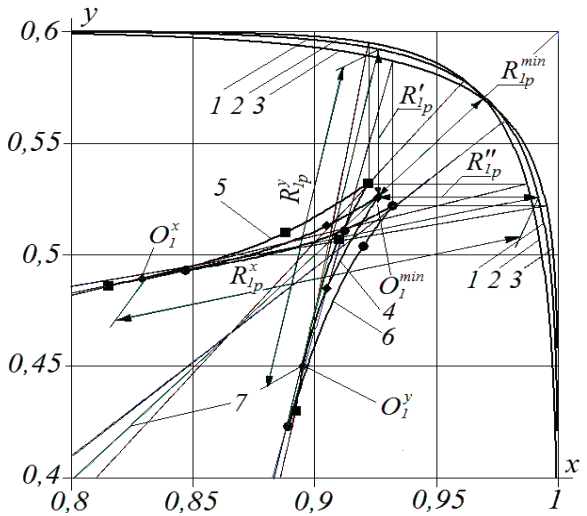

Figure 5.3. Contours of the angular zones of the beakers for different versions of the SPF: 1 - 3 – respectively for the contours $y_{13} = f(x)$ (Table 5.1); 4 - 6 – the deviation of the centers of the radii of curvature from the minimum with the growth of the radii in the direction of the bottom and the wall, respectively, for the contours 1 - 3; 7 – bisector of the angle between the bottom and the wall of the matrix

Curves 2 and 3 with a minimum of $R_{1p}{}^{min} = 0.060$, are characteristic for angular contours of beakers with SPF with the presence or absence of lubricant, R'_{1p} and R''_{1p} exceed R^{min}_{1p} by 3...18 %; the radii of curvature R^y_{1p} and R^x_{1p} in 2.5...3.0 times exceed R^{min}_{1p}, and their centers are spaced from the bisector 7 at distances equal to, respectively: 0.052 and 0.045 for the contour 2; 0.048 and 0.033 for the contour 3.

Table 5.1. Calculated values of parameters linking of angles of beakers in SPF

Function of the beaker contour	Minimum radius of curvature, r_1^{min}	Distance from the center of reference r_1^{min} to the contour		Radii of curvature (see Fig. 5.3)	
		bottom radius, R'_{1p}	wall radius, R''_{1p}	R^{y}_{1p}	R^{x}_{1p}
$y_1=0.6\left(1-x^{23.6}\right)^{1/13.2}$	0.063	0.065	0.066	0.167	0.168
$y_2=0.6\left(1-x^{32}\right)^{1/9}$	0.063	0.047	0.065	0.158	0.178
$y_3=0.6\left(1-x^{15}\right)^{1/19}$	0.060	0.071	0.062	0.181	0.150

It should be noted that:

1) contours with $R_{1p}^{min} < 0.03$, are achievable in practice, if in the SPF there was a preliminary pulling operation with a rigid punch;

2) the contours 1 - 3 in Fig. 5.3 can be formed for beakers with an initial thickness $S_0 \le R_1/3$ [67] that is for our case: $S_0 \ge 2$ mm.

An analytical model of superplastic forming of spherical shells by the pressure of a gas medium created during the sublimation of sublimate agent in the die cavity is developed. It is shown that the control of the pressure of the gaseous medium can be effectively performed by a corresponding change in the forming temperature relative to the sublimate agent sublimation temperature. The correspondence of the velocity behavior of shell superplastic forming to theoretically calculated values according to the developed model was experimentally confirmed.

In the case of superplastic forming of shells, the variability of walls thickness can be reduced by creating an uneven temperature

field along the workpiece surface during forming. In particular, SPF spherical shells are advisable to perform with simultaneous sublimation of sublimates covered on the central zones of the blank. The regulation of the thermally unstable coatings sublimation intensity should be carried out by changing the partial pressure over the sublimate, which changes the temperature and, consequently, the intensity of its sublimation. The sublimate sublimation temperature should be much lower than the SPF temperature. Sublimation of coating should begin upon reaching the height of the formed shell equal 20…30 % of the final shell height.

The contours of a sheet blank at all stages of superplastic forming can be approximated by curves of universal equations known to be a “superformula”, or “superellipse”. The values of indices this equation comprises allow describing the superplastic metal properties of a blank at a qualitative level, as well as the shape of this blank, the stages of plastic-forming and presence of additional operation for regulation of the flow of deformed metal. Geometrical contour of shells at the initial SPF stage can vary from spherical to parabolic or ellipsoid. Presence of lubrication between the die and shell promotes an increase of the curvature radius in these sections at the second stage of SPF.

6. EFFECT OF BLANK CURVATURE AND THINNING ON SHELL STRESSES AT SUPERPLASTIC FORMING

In engineering analysis of the stress-strain state and the power parameters of SPF the Laplace equation is usually used (4.1).

When analyzing the SPF process forming zones of blanks with a uniform or predetermined wall thickness that are free from contact with the stamp surface are often represented as spherical surface areas with an uneven (sometimes even) wall thickness [1, 10, 22–24, 68–69]. Such approach simplifies the determination of $R_1$and R_2 and, therefore, further calculations of stresses and forces. However, actual contours of the shells differ from spherical ones [25–27, 58, 60, 70]. This frequently requires to apply compensating elements in the system "deformable medium - blank" [28, 29, 71, 72] and introduces margins of error in the calculations, stipulating the need for their improvement.

Radii of curvature of free forming surfaces of the shells depend on the temperature, degree, strain rate, and superplastic properties of the material of the blanks. The principal radii of curvature R_1, R_2 are determined from various formulas that approximate experimental data. The distinction of the approach we are developing, is the assumption, that the most universal formula approximating the contour of a deformable blank at all stages of SPF is Lame's superellipse (4.3) [18, 19, 30, 53, 54, 73]. In this case the relative radii of curvature will be determined by the formulas (5.3), (5.4).

Taking into consideration formula $\sigma_m/r_1 + \sigma_\theta/r_2 = p/S$, derived from the expression (4.1), the relative radii of curvature $r_m = r_1/r$ and $r_\theta = r_2/r$ are determined as:

$$r_m = \frac{\left[1+(bp/q)^2 a^{-2p/q} x^{2(p-2)}\left(a^p - x^p\right)^{(1-q)/q}\right]^{3/2}}{-(bp/q)a^{-p/q}x^{p-2}\left(a^p - x^p\right)^{(1-2q)/q}\left[(p-1)\left(a^p - x^p\right)+((q-1)/q)px^p\right]};$$

$$r_\theta = -ba^{-p/q}\left(a^p - x^p\right)^{1/q}\left[1+(bp/q)^2 a^{-2p/q} x^{2(p-1)}\left(a^p - x^p\right)^{(2-2q)/q}\right]^{1/2}.$$

In the previous chapter, it was shown that for SPF domes from blanks of variable thickness (BVT) and with different superplastic properties, the radii of curvature R_{1p}, R_{2p} differ significantly from the radius of the spherical cover; they can be infinitely large and have extrema along the shell contour. Attention should be paid to the correlation between the change in the values of R_{1p}, R_{2p} r_m, r_θ and the thinning of the workpiece at SPF [68, 69, 74].

This chapter examines the relationship between principal stresses, radii of curvature, and shell thinning in SPF spherical domes to correct calculations of process force parameters.

To estimate the effect of the blank thickness on the stress state of the shell during the SPF, we used previously obtained experimental data and data from other authors [18–20, 25, 26, 58, 60, 75-77]. Thinning, i.e. the relative distribution of thickness $z = S / S_0$ along the relative radius of the base x of shells with a relative height of $y = 1$ was approximated by the equations presented in Table 6.1 for different materials (see Table 1.1).

On the basis of equation (6.1) and von Mises criterion, in works [19, 31, 74, 75] dependences convenient for analyzing the influence of the curvature of shell contours on the distribution of principal stresses σ_1, σ_2, σ_m, σ_θ and their intensities σ_e were obtained. For the relative values of the thickness (see Table 6.1) and the radii of curvature of the shells, these equations take the following form:

$$\sigma_1 = {pR_{2p}}/{2z}, \quad \sigma_2 = \left(2 - {R_{2p}}/{R_{1p}}\right)$$
$$\sigma_m = {pr_\theta}/{2z}, \quad \sigma_\theta = \left(2 - {r_\theta}/{r_m}\right){pr_\theta}/{2z}, \tag{6.1}$$

$$\sigma_e = {pR_{2p}}/{2z}\left[\sqrt{\left({R_{2p}}/{R_{1p}}\right)^2 - 3\left({R_{2p}}/{R_{1p}}\right) + 3}\right]$$
$$\sigma_e = \left({pr_\theta}/{2z}\right)\left[\sqrt{\left({r_\theta}/{r_m}\right)^2 - 3\left({r_\theta}/{r_m}\right) + 3}\right]. \tag{6.2}$$

Table 6.1. Formulas of approximation of the shell thickness at SPF

Shell parameters	Approximating function
alloy *AMg6* (analogs: *A95456*, *A95556* according to UNS, USA), blanks of variable thickness, t = 0,38	$z_2 = -1.94x^4 + 5{,}03x^3 - 3{,}31x^2 + 0{,}38x + 0{,}25$
alloy *Sn-38 %Pb*, t = 0,60	$z_3 = 1{,}09x^4 - 0{,}93x^3 + 0{,}17x^2 + 0.05x + 0{,}43$
alloy *Sn-38 %Pb*, t = 0,25	$z_4 = 0{,}88x^4 - 0{,}80x^3 + 0{,}44x^2 + 0{,}06x + 0{,}24$
alloy *AlMg5* DIN 1725 (analogs: *ALMG5*, ER 5356 / AWS A5.10), t = 0,42	$z_5 = 1{,}25x^4 - 1{,}82x^3 + 1{,}16x^2 + 0{,}00x + 0{,}23$

Assume that the shell contour is part of a sphere ${R_{2p}}/{R_{1p}} = 1$, and the shell thinning is uniform (z = 0.5), formula (6.2) is simplified to the following form:

$$\sigma_o = {}^{p}/_{2z}\text{, i. e. } \sigma_o = pR_{2p}$$

$$\sigma_o = {}^{pr_\theta}/_{2z}\text{, i.e. } \quad \sigma_o = pr_\theta . \tag{6.3}$$

Fig. 6.1a shows the distribution of the ratio of principal stresses σ_1 / σ_2, σ_θ / σ_m along the radius of the shells base. The calculations did not take into account the presence of the interface radius of the deformable shell and the flange, i.e. in the interval $x = (0.95...1.0)r$, the calculated data were unreliable and are not shown in the graphs.

For superplastic babbitt *Sn*-38%*Pb* with $t = 0.6$, the principal stresses are approximately equal (margin of error does not exceed 18 %). With the deterioration of superplastic properties in alloys, the calculated values of σ_2 and σ_θ prevail over the values of σ_1 and σ_m due to a significant increase in the radius of curvature, especially for babbitt with $t = 0.25$.

In blanks of variable thickness the distribution ${}^{\sigma_2}/_{\sigma_1} = f(x)$, ${}^{\sigma_\theta}/_{\sigma_m} = f(x)$ has the form of the parabola with a minimum in the range $x = 0.6...0.7$, i.e. in the places of interface of the central and peripheral zones of the blank with variable thickness.

At the intersection points of curves 1–4 with ordinate ${}^{\sigma_2}/_{\sigma_1} = 1$, ${}^{\sigma_\theta}/_{\sigma_m} = 1$, the contours of the shells coincide with the contour of the sphere. For babbitt shells with $t = 0.6$ and blanks of variable thickness, there are two such points in each one: ${}^{\sigma_2}/_{\sigma_1} = 0{,}99$, ${}^{\sigma_\theta}/_{\sigma_m} = 0.09$ and 0.62, 0.27, and 0.95, respectively. Babbitt shells with $t = 0.25$ and *AlMg*5 alloy have the ordinate ${}^{\sigma_2}/_{\sigma_1} = 1$, ${}^{\sigma_\theta}/_{\sigma_m} = 1$ at $x = 0.09$ and 0.44, respectively.

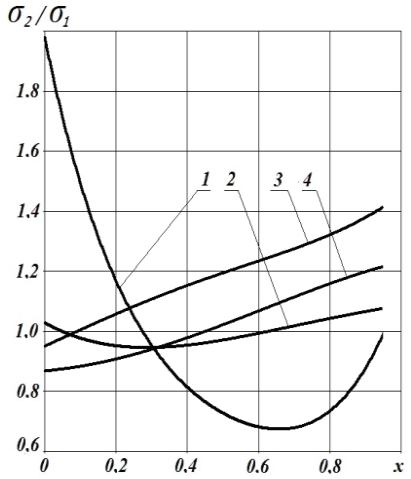

a)

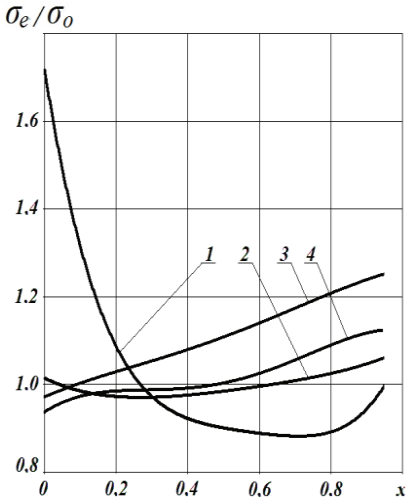

b)

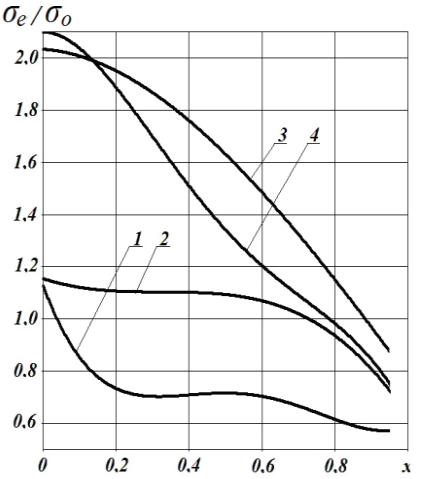

c)

Fig. 6.1. Distribution of the ratios of the principal stresses and effective stresses (stresses intensities) along the relative radius of the base of the shells from:
1 – *AMg6,* blanks of variable thickness;
2 – *Sn-38 %Pb* alloy with $t = 0.60$;
3 – *Sn-38 %Pb* alloy with $t = 0.25$;
4 – *AlMg*5 alloy

The differences in σ_θ and σ_m values along the contour of the shells determine the stress intensity (effective stresses) values σ_e, which differ from the similar parameters of σ_o for spherical shells (Fig. 6.1b). With the observed geometric similarity of the

corresponding graphs in Fig. 6.1a and Fig. 6.1b spread of σ_e/σ_o values for all shells is less than the range of σ_θ/σ_m values. With the margin of error of no more than 10%, it can be confirmed that it is acceptable to calculate the intensity of the stresses in the babbitt shells with $t = 0.60$ assuming that its contour is spherical and the equality $\sigma_1 = \sigma_2$, $\sigma_\theta = \sigma_m$.

However, for babbitt shells with $t = 0.25$ and *AlMg*5 alloy, the deviations σ_2/σ_1, σ_θ/σ_m and σ_e/σ_o are more significant: σ_2/σ_1, σ_θ/σ_m = 0.95...1.41 and 0.84...1.22, σ_e/σ_o = 0.97...1.25 and 0.93...1.13 respectively. In the shells from BVT, the minima of σ_e/σ_o and σ_2/σ_1, σ_θ/σ_m are reached in some places of the contour and make 0.88 and 0.66.

In some works [1, 10, 22, 32, 75, 77], when determining the power parameters of SPF, the contour sphericity and uniformity of the shells thinning were simultaneously assumed. According to our calculations, such assumptions lead to the fact that even in babbitt shells with a high level of superplastic properties (t = 0.60), the deviation of σ_e/σ_o values from a unity reaches + 0.15 ÷ - 0.26, i.e. margin of error reaches 41 % (Fig. 6.1c). For shells from blanks of variable thickness, the range of deviations is even greater: + 0.14 ÷ - 0.43 (margin of error – 57 %). In the pole sections of domes made of *AlMg*5 alloy and babbitt with $t = 0.25$, values $\sigma_e/\sigma_o > 2$, and in the areas of blank pressing, σ_e/σ_o = 0.76; 0.87, i.e. margin of error of calculation reaches 130 %.

Hence, the graphs in Fig. 6.1c show unacceptability for the calculations of the assumption about the uniformity of blanks thinning at SPF.

7. NICKEL-BASED SLAG-REMELTED SUPERALLOY FOR DIE-TOOL SUPERPLASTIC FORMING AND ISOTHERMAL STAMPING TI-ALLOYS

Using isothermal die forging and SPF efficiency for the forgings from Ti-based alloys production is mostly determined by the performance properties of the die tool. It is necessary to take into account a number of specific requirements for such dies production [1–6, 78–83]. The main requirements are the required strength margin at the forming temperature, surface oxidation lack for the die material and abrasive and fatigue properties stability under prolonged exploitation at temperatures range (of) T = 800...1000 °C. These requirements are met by heat-resistant nickel-based superalloys dies made with high tungsten content [7, 8, 84, 85] or intermetallics as NiAl–Ni3Al [9–11, 86–88], which are widely used in aircraft industry for isothermal and superplastic deformation of forgings. The die tools manufacturing from these alloys is quite labour-intensive, as it includes melting in vacuum arc furnaces (marked as "VD") and complex thermomechanical and/or electroerosive die engraves processing [12–16, 89–93]. Typical batch production for aircraft manufacturing can amount to thousands of forgings per year, while the die costs share in the forgings technological cost is low and offset by the isothermal forming advantages.

In other industries (shipbuilding, power engineering, and petrochemical industry) the batch production of titanium forgings, as a rule, does not exceed a thousand per year. In this regard, choosing die material for such conditions should be based on the improvement of both the forgings die forging, as well as die materials manufacturing. In the first case, the research purpose should be to reduce tool wear, electricity consumption, materials plastic properties

control and forming power modes [17–22, 94–99]. It is necessary to take into account the low technological performance of die materials, which is manifested in the fact that severe plastic deformation with high reduction leads to their fracture due to significant stresses arising in metals [23–27, 100–104]. In the second case, when choosing cheaper materials and their technologies, the use of mathematical modeling to assess the stress-strain and materials thermal state taking into account their plastic and thermophysical properties, accumulated damage and cracks becomes more common, with subsequently assessing their healing [28–32, 105–109]. Such materials can reduce the die-life to some extent, but this is quite acceptable with low batch production and frequent changes in the forgings range. The use of nickel-based superalloys as die materials for the Ti-based alloys forming is the most justified [33–35, 110]. Therefore, it is necessary to use cheaper options to produce tungsten-free die materials such as CrNi73CuBeTeAl (for example, not in vacuum arc furnaces, but by slag remelting process) and to evaluate their performance properties. Accordingly, this work purpose is to study the possibility of using the nickel alloy CrNi73CuBeTeAl (there are designations as ХН73МБТЮ or ЭИ 698), produced by electroslag remelting (ESR), as a die material for isothermal deformation.

The CrNi73CuBeTeAl-Sh alloy ("Sh" – marked as electroslag remelted) chemical composition, researched in this work, is shown in Table 7.1.

Waste of CrNi73CuBeTeAl-VD alloy ("VD" – vacuum arc remelted), which was tungsten-free and molybdenum-free, was used as the initial charge for smelting. This allowed to machine it with a blade tool, including on copy-milling machines. CrNi73CuBeTeAl-VD alloy in the form of pieces with dimensions not exceeding 60 mm was melted in an open induction furnace and cast into ingots with a 120-mm diameter. The single- or three-string electrodes were made of ingots by welding in argon medium using a CrNi73CuBeTeAl-VD alloy welding wire with a 3-mm diameter. The obtained electrodes

were converted into ingots with dimensions of 160 mm × 400 mm × 600 mm by electroslag remelting (ESR), which were cooled at 50 °C/min in a crystallizer thermoinsulated with a mullitosilicate felt 40-mm layer (Al_2O_3 ≥ 50 %, SiO_2 ≤ 47 %, $Al_2O_3 + SiO_2 = 97$ %, $Fe_2O_3 \leq 0.2$ %), then heated in an electric furnace to 900 °C, and kept 4 hours and cooled in it.

Table 7.1. CrNi73CuBeTeAl-Sh alloy chemical composition (wt. %)

C	Cr	Ti	Al	Mo	Nb	Ni	
0.06-0.07	14-15	2.35-2.55	1.5-1.6	2.8-3.0	1.9-2.0	Base	
Si	Mn	Fe	Ce	Pb	B	S	P
≤0.45	≤0.34	≤1.8	≤0.003	≤0.001	≤0.005	≤0.004	≤0.010

Isothermal forming in dies from the researched materials was simulated by tests for high-temperature cyclic creep. To do this, 20 mm high and 10 mm × 10 mm plan dimensions specimens were cut of the ingots, from their bottom, head and central zone, near the lateral surface and in the central axis zone. A 10 mm × 10 mm specimen's planes were placed parallel and perpendicular to the central axis of the ingots when cutting. Tests for high-temperature cyclic creep were performed in isothermal environment at a $T = 900$, 940 and 980 °C temperature with cyclic application in the direction of the specimen with 100, 200 and 300 MPa (N/mm^2) upsetting pressure. It was believed that the plane of force application is the die cavity working face. The forming velocities $V = 0.02$, 0.2 and 2.0 mm/s were chosen for the experiments, which provided loading of specimens with strain rates $\xi = 10^{-3} \cdots 10^{-1}$ s^{-1}.

After the specimen reached the ultimate plastic reduction at $\varepsilon = 1$ % height, the number of loading cycles (n) was recorded, which

was considered a dies life measure. Specimens were upset between flat dies of ЖС6У alloy (C = 0.15 %; Cr = 5.0 %; Co = 9.0 %; W = 11.7 %; Al = 5.9 %; Ti = 1.0 %; Mo = 1.1 %; Nb = 1.5 %; V = 1.0 %). Measurement accuracy: temperature ±10 ° C, upsetting pressure ± 16 MPa, specimens' height ± 0.01 mm. To compare cast CrNi73CuBeTeAl-Sh and CrNi73CuBeTeAl-VD alloys performances properties, specimens and die inserts from hot-deformed forging of CrNi73CuBeTeAl-VD alloy were also made and tested.

Cyclic creep tests have shown that ESR-alloy from the ingot bottom, i.e. from zone limited by its cross section and a 40-mm height, is inapplicable for dies, because it quickly wrinkles or cracks after 10-15 loading cycles. When studying the defective metal structure, slag and gating system remnants made of St3sp steel (analogs: Fe37-3FN, S235) were found in it. In the future, it was decided to remove the bottom part of all ESR ingots intended for the dies manufacturing with the volume determined by gating system remnants.

Studies of the flat ESR ingots porosity have shown that most microcavities during casting are shifted to the top part up to the ingot central axis, and the defect zone size depends on the remelting electrodes cross section. For single-string electrodes with 113-cm^2 cross-sectional area, the defective zone extends from the top to the ingot central zone at a 30-45 mm distance; for three-string electrodes with 340-cm^2 cross-sectional area – at up to 90-mm distance. The residual deformation exceeding 1 % for test specimens cut from defective zone was recorded after 24-40 loading cycles, which is unacceptable for the dies. In this regard, before cutting the billets for the dies the ESR ingots top part was removed at the 90-mm distance from the ingot top end.

At p = 300 MPa upsetting pressure, T = 940 °C temperature and V = 0.2 mm/s forming velocity, the alloy specimens cut near the lateral surface of the ingot central part with the working face parallel to the ingot central axis, have withstood maximum number of loading cycles (n_c = 272...285) to percent reduction by ε = 1 % or 3 %. In cases where

the die working face was perpendicular to the ingot central axis, the specimens cut from the lateral surface were upset to $\varepsilon = 1$ % for $n_c = 253...268$ cycles, while for specimens cut from the central zone, the test results were the same. Therefore, further tests of CrNi73CuBeTeAl-Sh alloy were performed on specimens cut from the lateral surface, with a working face parallel to the ingot central axis.

Fig. 7.1 shows the temperature and upsetting pressure effect on the number of loading cycles n_c, which causes the specimens upsetting to $\varepsilon = 1$ % at $V = 0.02...2.0$ mm/s deformation velocities. The electroslag remelting metal is inferior in efficiency of vacuum arc remelting alloy. Exceeding the number of loading cycles for vacuum arc remelting alloy in comparison with electroslag alloy is 7...9 % at $p = 200$ MPa and 300 MPa upsetting pressure, and 12...14 % at 100 MPa. With increasing the upsetting pressure from 100 MPa to 300 MPa the specimens upset accelerates, moreover with the greatest intensity it happens at $T = 980$ °C: with increasing upsetting pressure by 100 MPa, the alloy efficiency decreases to $n_c = 125$-140 loading cycles. However, with increasing the upsetting pressure p from 200 MPa to 300 MPa at temperatures 940 °C and 980 °C, the alloy upset intensity decreases by 30-40 cycles.

The specimens performances properties (efficiency) is determined more by the change in pressure than the testing temperature, but in some cases that interested us, for example, at $n_c = 400$ loading cycles within 100...140 MPa at 900...940 °C, the effect of p and T on n is the same. At the $V = 0.02$ mm/s deformation velocity (Fig. 7.1a), the dependences $n_c = f(T; p)$ have qualitatively the same form, as at $V = 0.2$ mm/s (Fig. 7.1b). However, the ultimate deformation $\varepsilon = 1$ % in the specimens is fixed at a significantly greater number of loading cycles than at $V = 0.02$ mm/s. When decreasing deformation velocity, the number of load cycles increases for “VD” alloy by 80-120 cycles, for ESR (“Sh”) alloy – by 70-125 cycles in the entire temperature range and at any upsetting pressure. A close

percentage ratio in the performance of CrNi73CuBeTeAl-VD and CrNi73CuBeTeAl-Sh alloys specimens, i.e. 8...15 %, is observed. But in absolute terms the increase of the loading cycles with deformation velocity decrease for VAF ("VD") alloy, in comparison with "Sh" alloy, is more significant, especially at T and p small values, and reaches 100 loading cycles at p = 100 MPa and T = 900 °C.

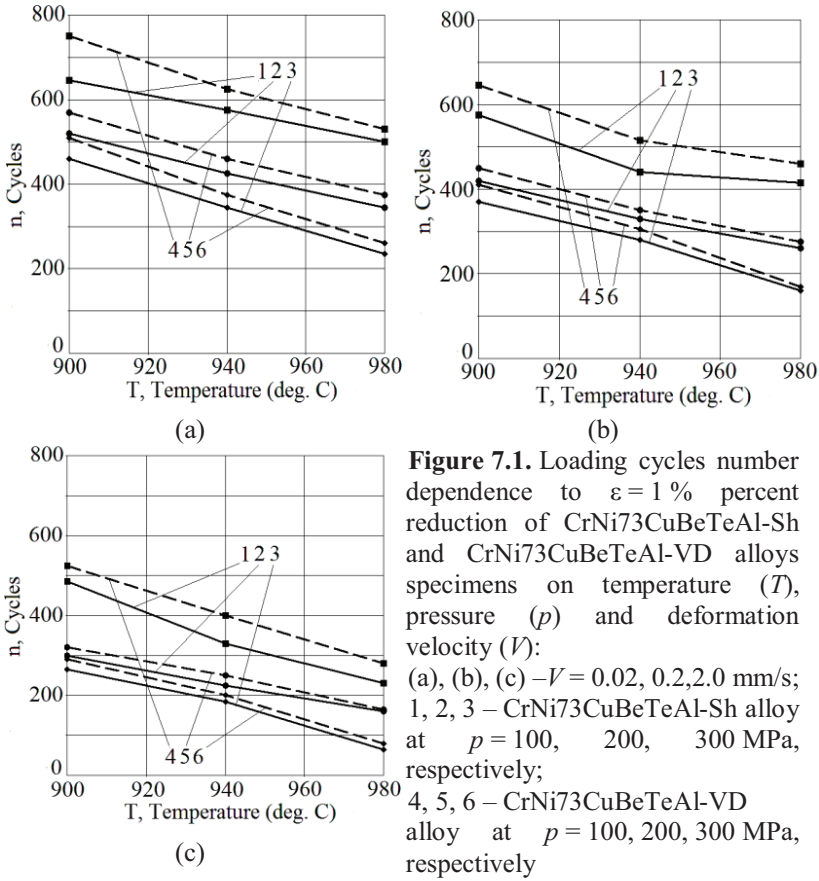

Figure 7.1. Loading cycles number dependence to ε = 1 % percent reduction of CrNi73CuBeTeAl-Sh and CrNi73CuBeTeAl-VD alloys specimens on temperature (T), pressure (p) and deformation velocity (V):
(a), (b), (c) – V = 0.02, 0.2,2.0 mm/s;
1, 2, 3 – CrNi73CuBeTeAl-Sh alloy at p = 100, 200, 300 MPa, respectively;
4, 5, 6 – CrNi73CuBeTeAl-VD alloy at p = 100, 200, 300 MPa, respectively

From the viewpoint of the forging processes productivity increase, the deformation velocity at specialized presses for isothermal

die-forging is often increased to a maximum, i.e. up to 2.0 mm/s. Fig. 7.1c shows how negatively it affects the die-tool. At 300 MPa upsetting pressure and 980 °C temperature, the maximum number of specimens loading cycles does not exceed 100, even for vacuum-arc remelting specimens. This is completely unacceptable for such processes, because in these cases it is better to make products by machining. The ultimate deformation of the die crumpling equal to $\varepsilon = 1$ %, provides, for example, the allowance on the blade airfoil with 10-mm thickness only 0.1-mm high. In some cases, forgings with this allowance can not be further processed by EDM to the blade final size, so often tool shops require forgings with at least 0.3 mm tolerances per side. In this case, the ultimate die deformation increases to $\varepsilon = 3$ %.

Thus, it is interesting how much the die life will increase at the restriction of deformation to $\varepsilon = 3$ %. The effect of upsetting temperature and pressure on the loading cycles number n_c, which causes the specimens upset to $\varepsilon = 3$ % is shown on Fig. 7.2. The Ti-alloys isothermal die forging is most often a cost-effective operation at the die life near 400 forgings or more. The graphs in Fig. 7.2 show that at a deformation rate of 2.0 mm/s and a draft pressure of 200 and 300 MPa, the dies still sag at $n_c \leq 400$ cycles, and a pressure of 100 MPa even at T = 90 °C is not suitable for stamping alloyed titanium alloys.

In this case, the die forging should be carried out with low deformation velocity (0.02...0.2 mm/s), but the die life will obtain the range of 420-550 forgings.

The obtained results were approximated by equations acceptable for further calculations, according to which it is possible to determine the maximum allowable process modes of isothermal die forging which provide a predetermined die life (in loading cycles numbers n_c). Given the linear nature of the graphs, many variables linear functions were chosen. These independent variables were the upsetting pressure p (MPa), the deformation temperature

T (°C), the deformation velocity V (mm/s) and the allowable residual deformation ε (%). The function was obtained:

$$n_c = -2.51 \cdot p - 4.46 \cdot T - 85.13 \cdot V + 51.61 \cdot \varepsilon + 4904.85 \quad (7.1)$$

according to which the temperature-force parameters of deformation for other indicators n_c i ε were predicted (Fig. 7.3).

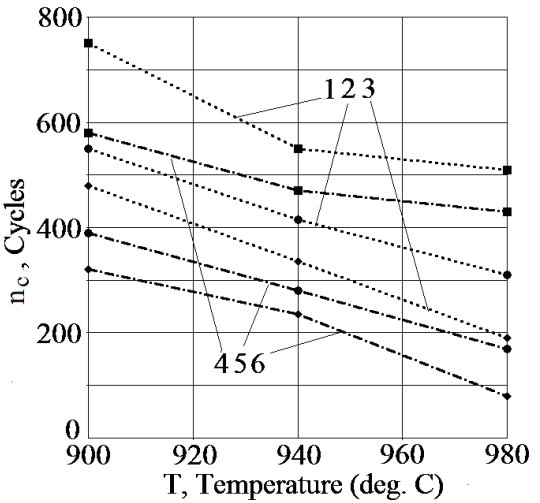

Figure 7.2. Loading cycles number dependence to ε = 3 %percent reduction of CrNi73CuBeTeAl-Sh alloy specimens on temperature (T), pressure (p) and velocity of deformation (V):
1, 2, 3 – V = 0.02 mm/s at p = 100, 200, 300 MPa, respectively;
4, 5, 6 – V = 2.0 mm/s at p = 100, 200, 300 MPa, respectively

The increase in the deformation velocity from 0.02 to 0.2 mm/s changes the graphs 1, 2 and 4, 5 rather slightly, and the difference of the pressure at the same temperature is 5…7 MPa. This difference becomes significant with increasing V value from 0.2 to 2.0 mm/s and reaches 60…70 MPa, i.e. increases by one order. Comparing the

graphs, we can conclude that, for example, at $V = 0.2$ mm/s and $T = 900$ °C the die life of $n_c = 500$ forgings can be achieved by die forging with a pressure not exceeding 190 MPa. If die life of $n_c = 300$ forgings is sufficient, the deformation temperature can be increased to 945 °C or to increase the upsetting pressure to 265 MPa at $T = 900$ °C.

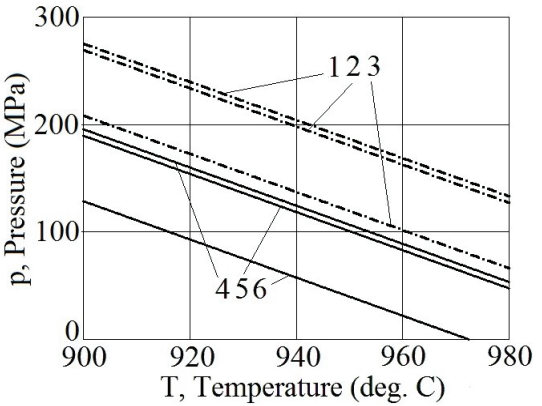

Figure 7.3. Analytically determined relation between upsetting pressure and temperature for providing a predetermined die life n_c at $\varepsilon = 2$ % for CrNi73CuBeTeAl-Sh alloy: 1, 2, 3 – $n_c = 300$ forgings at $V = 0.02$, 0.2, 2.0 mm/s, respectively; 4, 5, 6 – $n_c = 500$ forgings at $V = 0.02$, 0.2, 2.0 mm/s, respectively

Technologists often design die forging processes with a constant maximum allowable deformation of the die face, i.e. for $\varepsilon = \text{const}$. In this case, for $\varepsilon = 1$ %, the approximation equation is simplified to the form:

$$n = -1.23 \cdot p - 2.25 \cdot T - 95.96 \cdot V + 2829.42 \qquad (7.2)$$

Fig. 7.4 shows the change in the maximum allowable upsetting pressure depending on the die forging temperature, if at 1.0 mm/s deformation velocity it is necessary to ensure the die life of 300 and 500 forgings to restore the die. If we compare the graphs in Fig. 7.3 and Fig. 7.4, we can see that for $n_c = 300$ forgings can be forged at $T = 900$ °C with a 325-MPa maximum pressure at $V = 1.0$ mm/s, and 210 MPa at $V = 2.0$ mm/s. If the die life must be increased to 500 forgings at $T = 900$ °C, then the maximum upsetting pressure should be reduced from 170 MPa to 125 MPa. Such pressure values at the above-mentioned die forging temperatures can usually be only in sizing or flattening finishing operations of forgings that have already been forged.

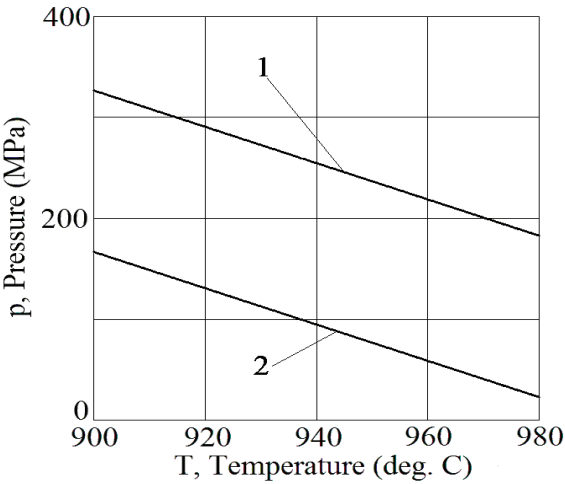

Figure 7.4. Analytically calculated relation between upsetting pressure and temperature to provide a predetermined die life n_c at $V = 1.0$ mm/s for CrNi73CuBeTeAl-Sh alloy: 1, 2 – $n_c = 300$ and 500 forgings, respectively

Taking into account the performed research, we made and tested dies from CrNi73CuBeTeAl-VD and CrNi73CuBeTeAl-Sh alloys in the form of inserts with 150 mm × 150 mm overall dimensions with a working face depth up to 65 mm, by cutting on lathe and milling machine from the lateral surface side of the ESR ingot central zone and from the side of "VD" alloy forging face. The inserts were installed in the die block located on a hydraulic press of PA2638 model with a 6.3 MN nominal force, and under isothermal conditions at 940 °C temperature were used for die forging with titanium VT3-1 alloy forgings closed upsetting (Fe = 0.2...0.7 %, Si = 0.15...0.4 %; Cr = 0.8...2 %; Mo = 2...3 %; Ti = 85.95...91.05 %; Al = 5.5...7 %) using ЭВТ-24 grease (lubricating and heat-insulating coating based on an aqueous glass powders dispersion system and colloidal solid lubricating particles for Ti-alloys hot forging with a 850...1000 °C operating temperature range). The press worked in the mode of "constant force", which provided the forming pressure within 280…310 MPa and the $\xi = 6 \cdot 10^{-1} \ldots 10^{-2}$ s^{-1} strain rate. After the manufacture of 40 forgings, the die insert face upsetting was 0.11 mm and 0.09 mm for CrNi73CuBeTeAl-Sh and CrNi73CuBeTeAl-VD alloys, respectively.

CONCLUSION

An analytical model of superplastic forming of spherical shells by the pressure of a gas medium created during the sublimation of sublimate agent in the die cavity is developed. It is shown that the control of the pressure of the gaseous medium can be effectively performed by a corresponding change in the forming temperature relative to the sublimate agent sublimation temperature. The correspondence of the velocity behavior of shell superplastic forming to theoretically calculated values according to the developed model was experimentally confirmed.

In the case of superplastic forming of shells, the variability of walls thickness can be reduced by creating an uneven temperature field along the workpiece surface during forming. In particular, SPF spherical shells are advisable to perform with simultaneous sublimation of sublimates covered on the central zones of the blank. The regulation of the thermally unstable coatings sublimation intensity should be carried out by changing the partial pressure over the sublimate, which changes the temperature and, consequently, the intensity of its sublimation. The sublimate sublimation temperature should be much lower than the SPF temperature. Sublimation of coating should begin upon reaching the height of the formed shell equal 20…30 % of the final shell height.

The contours of a sheet blank at all stages of superplastic forming can be approximated by curves of universal equations known to be a “superformula”, or “superellipse”. The values of indices this equation comprises allow describing the superplastic metal properties of a blank at a qualitative level, as well as the shape of this blank, the stages of plastic-forming and presence of additional operation for regulation of the flow of deformed metal. Geometrical contour of

shells at the initial SPF stage can vary from spherical to parabolic or ellipsoid. Presence of lubrication between the die and shell promotes an increase of the curvature radius in these sections at the second stage of SPF.

It is established that different versions of the SPF cause different radii of curvature of the shell contours that differ significantly from the radius of the spherical segment. It is shown that the radius of the linking between the bottom and the wall of the beakers increases along the contour of the shell from a minimum in the sides of the bottom and walls, and its center moves away from the bisector of the angle of the beaker along two branches of the parabola.

Simulation of the processes of super-plastic deformation with the help of optically transparent non-linear viscous block-copolymers, on the basis of diene and vinyl-aromatic carbohydrates of polar softener and achromatic stabilizer makes it possible to observe physically the process of deformation along the entire process of samples deforming. By means of a coordinate grid, placed upon the diametric plane of such samples and video recording of the process it is possible to analyze quantitative and qualitative and qualitative changes along the entire volume at any time span.

The principal stresses, in particular the tangential stress, depend on the principal radii of curvature. The intensity of stresses also depends on the thinning of the shells at superplastic forming. The higher the level of superplastic properties of the blank material, the less the main stresses and their intensity depend on the difference between the principal radii of curvature. When calculating the power mode of SPF shells, the assumption of uniform thinning of the blank during forming is unacceptable, since margin of error of the calculations can reach 130 %.

The fundamental possibility to use the tungsten-free CrNi73CuBeTeAl alloy manufactured of both vacuum arc remelting and electroslag remelting as die tool material for isothermal die forging is shown. It will be efficient to use such dies for isothermal die

forging blades made of Ti-alloy with rather big allowance on the overall sizes, which assumes residual dies upsetting $\varepsilon = 1.0\text{-}3.0$ % during exploitation. If the forging temperature does not exceed 940 °C, the die life for these forgings can be increased to 600-700 loading cycles. It will be quite effective to use such dies for isothermal sizing of Ti-alloys compressor and aircraft turbine engine blades, which is carried out at $T = 850\ldots950$ °C and $p = 100\ldots150$ MPa. In this case, the die life will be 400…550 cycles of sizing. By reducing the complexity of ingot smelting and the ability to make the working face on copiers and milling machines instead of EDM, the dies manufacturing from ESP alloys will reduce the dies expenses in the blade forgings technological cost from 32 % to 20…22 %.

REFERENCES

1. Giuliano G. Superplastic Forming of Advanced Metallic Materials: Method and Applications, Oxford-Cambridge-Philadelfia-New Dehli, Woodhead Publishing Ltd., 2011, 377 p.

2. Bhoyar P. K. Futuristic Superplastic Forming Materials. International Journal For Administration in Management, Commerce and Economics (IJAMCE). 2015, pp. 284-289, www.ijamce.org/pdf/jan48.pdf.

3. Golenkov V. A., Dmitriev A. M., Kukhar V. D., Radchenko S. Yu., Yakovlev S. P. and Yakovlev S. S. Special technological processes and equipment for pressure treatment. Moscow, Engineering, 2004. 474 p.

4. Samekto H. and Roll K. Finite Element Analysis of Superplastic Forming Process Using LS-DYNA, 4th European LS-DYNA Users Conference, Metal Forming II, E II, 2003, 16 p., http://www.dynalook.com/european-conf-2003/finite-element-analysis-of-superplastic-forming.pdf.

5. Deshmukh P. V. Study of Superplastic Forming Process Using Finite Element Analysis, University of Kentucky Master's Theses, 2003, vol. 367, 97 p. https://uknowledge.uky.edu/ gradschool_ theses/367.

6. Balasubramanian M., Ramanathan K., and Senthilkumar V.S. Mathematical Modeling and Finite Element Analysis of Superplastic Forming of Ti-6Al-4 V Alloy in a Stepped Rectangular Die. Procedia Engineering, 2013, vol. 64, pp. 1209-1218, DOI: 10.1016/j.proeng. 2013.09.200.

7. Zakhariev I. Y. and Aksenov S. A. Influence of a Material Rheological Characteristics on the Dome Thickness during Free Bulging Test. Journal of Chemical Technology and Metallurgy,

2017, Vol. 52, Issue 5, pp. 1002-1007,
http://dl.uctm.edu/journal/node/j2017-5/27_16-149_Zakhariev_
1002-1007.pdf.

8. Bonet J., Gil A., Wood R. D., Said R., and Curtis R. V. Simulating superplastic forming. Computer Methods in Applied Mechanics and Engineering, 2006, vol. 195, issues 48–49, pp. 6580–6603, DOI: 10.1016/j.cma.2005.03.012.

9. Lee S., Tang J. S., and Chu C. L. Prior sheet buckling leading to wrinkling formation in a gas forming a V-trough with wavy bottom. Journal of Manufacturing Processes, 2016, vol. 21, pp. 101–106, DOI: 10.1016/j.jmapro.2015.12.001.

10. Jovane F. An approximate analysis of the superplastic forming of a thin circular diaphragm: theory and experiments. International Journal Mechanical Science, 1968, vol. 10, issue 6, pp. 409–427.

11. Anishchenko A.S. Izotermicheskaja i sverhplasticheskaja deformacija metallov. Saarbrücken: LAMBERT Academic Publishing, 2014, 129 p.

12. Zhang K. F., Wang G. F., Wu D. Z., Wang Z. R. Research on the controlling of the thickness distribution in superplastic forming. Journal of Materials Processing Technology, 2004, 151 (1-3), pp. 54-57, DOI: 10.1016/j.jmatprotec.2004.04.008.

13. Dutta A. Thickness-profiling of initial blank for superplastic forming of uniformly thick domes. Materials Science and Engineering, 2004, 371 (1-2), pp.79-81.

14. Jeyasingh J. J. V., Kothandaraman G., Sinha P. P., Nageswara B. R., Chennakesava A. R. Spherical dome formation by transformation of superplasticity of titanium alloys and titanium matrix composites. Materials Science and Engineering, 2008, A 478, pp. 397–401.

15. Cheong B. H., Lin J., Ball A. A. Modelling of hardening due to grain growth for a superplastic alloy. Journal of Materials Processing Technology, 2001, 119(1-3), pp.361–365.

16. Skuridin, B. V., Smirnov, O. M., Gusev, Ju. V., and Panfilova, O. V. . Deformirivanye Titanovyh Splavov v Usloviyah Sverhplastichnosti. Kuznechno-Shtampovochnoye Proizvodstvo, 1977, Vol. 12, pp. 35-38. (in Rus.).

17. Babu S. R., Kumar V.S., Karunamoorthy L., Reddy M.G., Investigation on the effect of friction stir processing on the superplastic forming of AZ31B alloy. Materials and Design, 2014, vol. 53, pp.338-348.

18. Marinho E. P., Ribeiro F. C. and Batalha G. F. ABCM Symposium in Mechatronics. Control Systems, ed SCAAlfaro, JMST Motta and VJDeNeg (Rio de Janeiro: ABCM – Brazilian Society of Mechanical Sciences and Engineering), 2012, vol. 5 Section II, pp. 380-389.

19. Divya H. V., La.xmana N. L., Niranjan H. M., Vasundhara M. G. and Yogesha B. International Journal of Advances in Engineering & Technology, 2013, vol. 6(4), pp. 1829–1835. 20. Furushima T. and Manabe K. Journal of Materials Processing Technology, 2007, vol. 191(1), pp. 59–63.

21. Furushima T. and Manabe K. Journal of the Chinese Society of Mechanical Engineers, Transactions of the Chinese Institute of Engineers – Series C, 2010, vol. 31(2), pp. 99–105.

22. Milenin A., Kustra P., Furushima T., Du P. and Nemecek J., Journal of Materials Processing Technology, 2018, vol. 262. pp. 65-74.

23. Kukhar V., Artiukh V., Prysiazhnyi A. and Pustovgar A., E3S Web of Conference, 2018 (HRC 2017), vol. 33, pp. 02031.

24. Kukhar V. V. Metallurgical and Mining Industry, 2015, vol. 6, pp. 122–132.

25. Kukhar V., Artiukh V., Serduik O. and Balalayeva E. Procedia Engineering, 2016, vol. 165, pp. 1693–1704.

26. Kukhar V., Prysiazhnyi A., Balalayeva E. and Anishchenko O. Modern Electrical and Energy System MEES'2017 (Kremenchuk: Kremenchuk Mykhailo Ostrohradskyi National

University, IEEE), 2017, pp. 404–407.

27. Kukhar V., Balalayeva E., Prysiaznyi A., Vasylevskyi O. and Marchenko I. MATEC Web of Conferences, 2018, vol. 178, pp. 02003.

28. Tandogan M. and Eyercioglu O. International Advanced Research Journal in Science, Engineering and Technology, 2017, vol. 4(12), pp. 62–73.

29. Jones J. J. and Mears L. Proceedings of the 2010 International Manufacturing Science and Engineering Conference MSEC 2010 (Erie, Pennsylvania: ASME), DRAFT-MSEC, 2010, p. 34144.

30. Langdon T. G. Journal of Materials Science, 2009, vol. 44, pp. 5998-6010.

31. Langdon T. G. Materials Science Forum, 2016, vol. 838(839), pp. 3–12.

32. Davis B. and Hryn J. Innovative forming and fabrication technologies: new opportunities. Final Report, 2007. www.ipd.anl.gov/anlpubs/2008/01/60753.pdf.

33. Lihui L., Kangning L., Cai G., Yang X., Guo C. and Bu G., Manufacturing Review, 2014, vol. 1(9), pp. 1–20.

34. Abu-Farha F. K. and Khraisheh M. K. Int. J. Sustainable Manufacturing, 2008, vol. 1(1/2), pp. 18–40.

35. Alabor E., Putman D., Reed R. C. Acta Materialia, 2015, vol. 95(15). pp. 428–442.

36. Tisza M. Materials Science Forum, 2005, vol. 473(474), pp. 135–140.

37. Abu-Farha F. K. and Khraisheh M. K. Int. J. Sustainable Manufacturing, 2008, vol. 1(1/2), pp. 18–40.

38. Tisza M. Materials Science Forum, 2005, vol. 473(474), pp. 135–140.

39. Pertence A. E. M. and Cetlin P. R. Journal of Materials Processing Technology, 1998. vol. 84, pp. 261–267.

40. Tekkaya A. E. Simulation of Metal Forming Processes

(In: Banabic D (eds) Formability of Metallic Materials, Engineering Materials, Springer, Berlin, Heidelberg), 2000.

41. Kukhar V., Artiukh V., Butyrin A. and Prysiazhnyi A. Advances in Intelligent Systems and Computing, 2018, vol. 692. pp. 201–211.

42. Grushko A. V., Kukhar V. V. and Slobodyanyuk Yu. O. Solid State Phenomena, 2017, vol. 265, pp. 114–123.

43. Ravindra Reddy P. V. R., Chandra Mohan Reddy G. and Radhakrishna Prasad P. International Journal of Modern Engineering Research (IJMER), 2012, vol. 2(4), pp. 2326–2330.

44. Korshak V. F., Shapovalov Y. A. and Vaselenko N. N. Metallofiz. Noveishie Tekhnol, 2015, vol. 37(12), pp. 1633–1642.

45. Rudskoi A. I. and Rudaev Ya. I. Mechanics of dynamic superplasticity of aluminum alloys. Sankt-Petersburg, Nauka, 2009, 218 p.

46. Sheikh-Ali Askar D. A Study of Deformation Mechanisms of Creep and Superplasticity in Zinc. PhD Thesis, McGili University, Montreal, Québec, Canada, 2004.

47. Tu Z. H., Shim V. P. W. and Lim C. T. International Journal of Solids and Structures, 2001, vol. 38(50–51), pp. 9267-9279.

48. Shams I. and Yano H. Scientific Reports, 2015, vol. 5, p. 16421.

49. Balalayeva E., Artiukh V., Kukhar V., Tuzenko O., Glazko V., Prysiazhnyi A. and Kankhva V. Advances in Intelligent Systems and Computing, 2018, vol. 692, pp. 220–235.

50. Kukhar V., Balalayeva E. and Nesterov O. MATEC Web of Conferences, 2017, vol. 129, p. 01041.

51. Artiukh V., Nikitchenko A., Ignatovich I. and Prykina L. IOP Conf. Ser.: Earth Environ. Sci., 2017, vol. 90, p. 012191.

52. Fuge M., Yumer M. E., Orbay G., and Kara L. B. Conceptual Design and Modification of Freeform Surfaces Using Dual Shape Representations in Augmented Reality Environments.

Computer-Aided Design, 2012, Vol. 44. pp. 1020-1032, DOI:10.1016/ j.cad.2011.05.009.

53. Tang C.Y., Fung K.Y., Lee E.W.M., Ho G.T.S., Siu K.W.M., and Mou W. L. Product Form Design Using Customer Perception Evaluation by a Combined Superellipse Fitting and ANN Approach. Advanced Engineering Informatics, 2013, vol. 27, pp. 386-394, DOI: 10.1016/ j.aei.2013.03.006.

54. Gielis J. A Generic Geometric Transformation that Unifies a Wide Range of Natural and Abstract Shapes. American Journal of Botany, 2003, vol. 90, Issue 3, pp. 333-338, DOI: 10.3732/ajb.90.3.333.

55. Caratelli D., Ricci P. E., and Gielis J. The Robin Problem for the Laplace Equation in a Three-Dimensional Starlike Domain. Applied Mathematics and Computation, 2011, Vol. 218, pp. 713-719, DOI: 10.1016/j.amc.2011.03.146.

56. Vasin R. A., Enikeev F. U., and Safiulin R. V. Mathematical Modeling of Superplastic Forming of a Long Rectangular Box Section. Material Scientific Forum, 1999, vol. 304-306, pp. 765-770, DOI: 10.4028/www.scientific.net/MSF.304-306.765.

57. Lechten J.-P., Patrat J.-C., and Baudelet B. Analyses Theorique et Experimentale du Gonflement Dans le Domaine de Superplasticite. Revue de Physique Appliquee, 1977, vol. 12, Issue 1, pp .7-14, DOI: 10.1051/rphysap:019770012010700.(in Fr.).

58. Hwang Y. M., Lin Y. K. and Altan T. Evaluation of Tubular Materials by a Hydraulic Bulge Test. International Journal of Machine Tools and Manufacturing, 2007, Vol. 47, Issue 2, pp. 343-351, DOI: 10.1016/j.ijmachtools.2006.03.009.

59. Vitu L., Boudeau N., Malécot P., Michel G., and Buteri A. Comparaison de Trois Modeles Pour le Post-Traitment de Mesures Issues du Test de Gonflement Libre de Tubes. 22-ieme Congres Francais de Mecanique, Lyon, 2015, pp. 67-78, http://documents. irevues.inist.fr/bitstream/handle/2042/57605/66389.pdf. (in Fr.).

60. Musaev E. A., Sheryshev A. E., and Sheryshev M. A. Technological Support for Production of Articles of Polymers by Free Thermoforming. Polymer Science, Series D, 2017, vol. 10, Issue 2, pp. 165-168, doi: 10.1134/S1995421217020150. (in Rus.).

61. Smirnov O. M. Metal Forming in Superplastic State, Moscow, 1979, Mashinostroenie, 184 p.

62. Ragab A.R. Thermoforming of Superplastic Sheet in Shaped Dies. Metal *Materials Technology*, 1983, vol. 10, Issue 1, pp. 340-348, doi: 10.1179/030716983803291262.

63. Rudskoy A.I., and Rudaev Y.I. Mekhanika Dinamicheskoy Sverhplastichnosti Aluminievyh Splavov, Sankt-Petersburg, 2009, Nauka, 218 p.

64. Smirnov O. M., Guk V. O., Tsepin M. A. and Anishchenko A. S. Sposoby Umenshenya Raznotolshchinnosti pri Pnevmoformovke Detaley v Rezhime Sverkhplastichnosti. Teorya i Tehnologya Obrabotki Metallov Davleniem, Moscow, MISIS, 1979, vol. 113, pp. 70-75.

65. Ceschini L. Superplastic Forming (SPF) of Materials and SPF Combined with Diffusion Bonding: Technological and Design Aspects / L. Ceschini, A. Africantov // Metallurgical Science and Technology, 1992, vol. 10 (3), pp. 41-55.

66. Yong H. Kim, Jung-Min Lee, S.S. Hong. Optimal design of superplastic forming processes. Journal of Materials Processing Technology, 2001, vol. 112(2–3), pp. 167–173. DOI: 10.1016/S0924-0136(00)00880-3.

67. Abhijit Dutta. Thickness-profiling of initial blank for superplastic forming of uniformly thick domes. Material Science and Engineering A., 2004, vol. 371(1–2), pp. 79–81. DOI: 10.1016/S0921-5093(03)00632-4.

68. Anishchenko A. S., Feofanov Yu. V., Bogun A. B. Hot expansion of precise ring forgings. Chemical and Petroleum Engineering, 1992, vol. 11, pp. 33–35.

69. Kukhar V., Balalayeva E., Nesterov O. Calculation Method and Simulation of Work of the Ring Elastic Compensator for Sheet-Forming. MATEC Web of Conferences, 2017, vol. 129, pp. 01041. DOI: 10.1051/matecconf/201712901041.

70. Balalayeva E., Artiukh V., Kukhar V., Tuzenko O., Glazko V., Prysiazhnyi A., Kankhva V. Researching of the Stress-Strain State of the Open-Type Press Frame Using of Elastic Compensator of Errors of "Press-Die" System. Advances in Intelligent Systems and Computing, 2018, vol. 692, pp. 220-235. DOI: 10.1007/978-3-319-70987-1_24.

71. Sadowsky A.J., Rotter A.M. Exploration of Novel Geometric Imperfection Forms in Buckling Failures of Thin-Walled Metal Silos under Eccentric Discharge. International Journal of Solids and Structures, 2012, vol. 50(5), pp. 781–794. DOI: 10.1016/j.ijsolstr.2012.11.017.

72. Deshmukh, Pushkarraj Vasant. Study Of Superplastic Forming Process Using Finite Element Analysis. University of Kentucky Master's Theses, 2003, Paper 367, 82 p. http://uknowledge.uky.edu/gradschool_theses/367.

73. Anishchenko A., Kukhar V., Artiukh V., Olga A. Superplastic forming of shells from sheet blanks with thermally unstable coatings. MATEC Web of Conferences, 2018, vol. 238, pp. 06006. DOI: 10.1051/matecconf/201823906006.

74. Anishchenko O. S., Kukhar V. V., Grushko A. V., Vishtak I. V., Prysiazhnyi A. H., Balalayeva E. Yu. Analysis of the Sheet Shell's Curvature with Lame's Superellipse Method during Superplastic Forming. Materials Science Forum, 2019, vol. 945, pp. 531–537. DOI: 10.4028/www.scientific.net/MSF.945.531.

75. Anishchenko A., Kukhar V., Artiukh V., Arkhipova O. Application of G. Lame's and J. Gielis' formulas for description of shells superplastic forming. MATEC Web of Conferences, 2018, vol. 238. pp. 06007. DOI: 10.1051/matecconf/201823906007.

76. Ohno T., Watanabe R., Nonomura T., Development of a Die Material for Isothermal Forging of Superalloys in Air, Transactions of the Iron and Steel Institute of Japan, 1987, vol. 27(1), pp. 34–41.

77. Boër C.R., Rydstad H., Schröder G. Choosing optimal forging conditions in isothermal and hot-die forging, J. Applied Metalworking, 1985, vol. 3, pp. 421–431.

78. Behrens B.A., Kazhai M., Prüb T., Potentials of Ceramic Die Materials for Isothermal Forging Purposes of a Titanium Alloy, Key Engineering Materials, 2014, vol. 611–612, pp. 202–211.

79. Montero R.E., Housefield L.G., Mace R.S. Isothermal and Hot-Die Forging, In Book: Metalworking: Bulk Forming, Volume 14A. S.L. Semiatin (eds.), ASM International, 2005.

80. Buchmayr B., Damage, Lifetime, and Repair of Forging Dies, Berg Huettenmaenn Monatsh, 2017, vol. 162, pp. 88–93.

81. Kukhar V., Balalayeva E., Hurkovska S., Sahirov Y., Markov O., Prysiazhnyi A. The Selection of Options for Closed-Die Forging of Complex Parts Using Computer Simulation by the Criteria of Material Savings and Minimum Forging Force, Advances in Intelligent Systems and Computing, 2020, vol. 989 pp. 325–331.

82. Nowotnik A., Nickel-Based Superalloys, In book: Reference Module in Materials Science and Materials Engineering, MATS, 2016, p. 02574.

83. Satyanarayana D. V. V., Eswara Prasad N. Nickel-Based Superalloys, In: Prasad N., Wanhill R. (eds.), Aerospace Materials and Material Technologies, Indian Institute of Metals Series, Springer, Singapore, 2017, pp. 199–228.

84. Jozwik P., Polkowski W., Bojar Z. Applications of Ni3Al Based Intermetallic Alloys - Current Stage and Potential Perceptivities, Materials, 2015, vol. 8(5), pp. 2537–2568.

85. Povarova K. B., Skachkov O. A. Preparation, Structure, and Properties of Ni3Al and NiAl Light Powder Alloys for Aerospace, Materials Science Forum, 2007, vol. 534-536, pp. 1585–1588.

86. Czeppe T., Wierzbinski S. Structure and mechanical properties of NiAl and Ni3Al-based alloys, International Journal of Mechanical Sciences, 2000, vol. 42(8), pp. 1499–1518.

87. Tarelnyk V.B., Gaponova O. P., Konoplyanchenko Ye. V., Yevtushenko N. S., Herasymenko V.O. The Analysis of a Structural State of Surface Layer after Electroerosive Alloying, II. Features of Formation of Electroerosive Coatings on Special Steels and Alloys by Hard Wear-Resistant and Soft Antifriction Materials, Metallofiz. Noveishie Tekhnol, 2018, vol. 40(6), pp. 795–815.

88. Efremenko V. G., Hesse O., Freidrich Th., Kunert M., Brykov M., Shimizu K., Zurnadzhy V., Suchmann P. Two-body abrasion resistance of high-carbon high-silicon steel: Metastable austenite vs nanostructured bainite, Wear, 2019, vol. 418–419, pp. 24–35.

89. Malinov L. S., Malysheva I. E., Klimov E. S., Kukhar V. V., Balalayeva E. Yu. Effect of Particular Combinations of Quenching, Tempering and Carburization on Abrasive Wear of Low-Carbon Manganese Steels with Metastable Austenite, Materials Science Forum, 2019, vol. 945, pp. 574–578.

90. Anishchenko A. S. Heat treatment effect on properties of deformed alloy type 36N, Metallovedenie i Termicheskaya Obrabotka Metallov, 1996, vol. 4, pp. 31–32.

91. Dragobetskii V., Zagirnyak V., Shlyk S., Shapoval A., Naumova O. Application of explosion treatment methods for production items of powder materials, Przeglad Elektrotechniczny, 2019, vol. 95(5), pp. 39–42.

92. Anishchenko A. S., Sosnovskij N. Yu. Rolling machines for washing machines bodies working, Kuznechno-Shtampovochnoe Proizvodstvo, 1993, vol. 11, pp. 27–28.

93. Puzyr R., Kukhar V., Maslov A., Shchipkovskyi Y. The Development of the Method for the Calculation of the Shaping Force in the Production of Vehicle Wheel Rims, International Journal of Engineering & Technology (UAE), 2018, vol. 7(4.3), pp. 30–34.

94. Yarymbash D., Kotsur M., Bezverkhnia Y., Yarymbash S., Kotsur I. Parameters determination of the trolley busbars by electromagnetic field simulation, In Proc. 2018 IEEE 3rd International Conference on Intelligent Energy and Power Systems (IEPS 2018), 2018-January, 2018, pp. 76–79.

95. Korol S. O., Moroz M., Korol S. S., Yelistratov V., Moroz O. Development of a Moderator of the Pump Controlled Drive for the Engine, 2019 IEEE International Conference on Modern Electrical and Energy Systems (MEES), Kremenchuk, Ukraine, 2019, pp. 30–33.

96. Kaplanov V. I., Prisyazhnyi A. G. Simulation of contact friction in the hot rolling of steel sheet, Steel in Translation, 2008, vol. 38(9), pp. 714–718.

97. Anishchenko A. S., Andryushchenko A. P. Rotary flaring of faceted flairs on pipe blanks, Soviet Engineering Research, 1991, vol. 11(5), pp. 95–97.

98. Kukhar V. V., Grushko A. V., Vishtak I. V. Shape Indexes for Dieless Forming of Elongated Forgings with Sharpened End by Tensile Drawing with Rupture, Solid State Phenomena, 2018, vol. 284, pp. 408–415.

99. Markov O., Gerasimenko O., Aliieva L., Shapoval A., Kosilov M. Development of a new process for expanding stepped tapered rings, Eastern-European Journal of Enterprise Technologies, 2019, vol. 2(1–98), pp. 39–46.

100. Hrudkina N., Aliieva L., Abhari P., Markov O., Sukhovirska L. Investigating the process of shrinkage depression formation at the combined radial-backward extrusion of parts with a flange, Eastern-European Journal of Enterprise Technologies, 2019, vol. 5(1–101), pp. 49–57.

101. Hrudkina N. S., Aliieva L. I., Modeling of cold extrusion processes using kinematic trapezoidal modules, FME Transactions, 2020, vol. 48(2), pp. 357–363.

102. Anishchenko A. S., Feofanov Y. V., Bogun A. B. Hot expansion of precise ring forgings, Khimicheskoe I Neftegazovoe Mashinostroenie, 1992, vol. 11, pp. 33–35.

103. Kukhar V., Kurpe O., Klimov E., Balalayeva E., Dragobetskii V. Improvement of the Method for Calculation the Metal Temperature Loss on a Coilbox Unit at the Rolling on Hot Strip Mills, International Journal of Engineering & Technology (UAE), 2018, vol. 7(4.3), pp. 35–39.

104. Trotsko O., Shlyk S. Development of the mathematical model for sheet blanks forming calculation using simulation in ANSYS software, In Proc. 2018 IEEE 13th International Scientific and Technical Conference on Computer Sciences and Information Technologies (CSIT 2018), 2018, vol. 1, pp. 169–172.

105. Oginskiy I. K. New approaches to the definition of power parameters of rolling based on finite volume method, Metallurgical and Mining Industry, 2011, vol. 7, pp. 20–26.

106. Chereches T., Lixandru P., Mazuru S., Cosovschi P., Dragnea D. Numerical simulation of plastic deformation processes from cast iron parts, Academic Journal of Manufacturing Engineering, 2014, vol. 12(2), pp. 29–36.

107. Shats'kyi I. P. Limiting equilibrium of a plate with partially healed crack, Materials Science, 2015, vol. 51(3), pp. 322-330.

108. Odenberger E.-L., Oldenburg M., Thilderkvist P., Stoehr T., Lechler J., Merklein M. Tool development based on modelling and simulation of hot sheet metal forming of Ti–6Al–4V titanium alloy, Journal of Materials Processing Technology, 2011, vol. 211(8), pp. 1324–1335.

109. Li Z., Qu H., Chen F., Wang Y., Tan Z., Kopec M., Wang K., Zheng K. Deformation Behavior and Microstructural

Evolution during Hot Stamping of TA15 Sheets: Experimentation and Modelling, Materials, 2019, vol. 12(2), p. 223.

110. Lypchanskyi O., Sleboda T., Zyguła K., Łukaszek-Sołek A., Wojtaszek M. Evaluation of Hot Workability of Nickel-Based Superalloy Using Activation Energy Map and Processing Maps, Materials, 2020, vol. 13(16), p. 3629.